MULTI-STAGE BUBBLE COLUMN HUMIDIFIER FOR THERMAL DRIVEN MECHANICAL COMPRESSION HUMIDIFICATION DEHUMIDIFICATION DESALINATION SYSTEM

BY

OBAIDALLAH MOHAMMAD ALI MUNTESHARI

A Thesis Presented to the

DEANSHIP OF GRADUATE STUDIES

KING FAHD UNIVERSITY OF PETROLEUM & MINERALS

DHAHRAN, SAUDI ARABIA

In Partial Fulfillment of the
Requirements for the Degree of

MASTER OF SCIENCE

In

MECHANICAL ENGINEERING

APRIL 2014

KING FAHD UNIVERSITY OF PETROLEUM & MINERALS
DHAHRAN 31261, SAUDI ARABIA

DEANSHIP OF GRADUATE STUDIES

This thesis, written by **OBAIDALLAH MOHAMMAD ALI MUNTESHARI** under the direction of his thesis adviser and approved by his thesis committee, has been presented to and accepted by the Dean of Graduate Studies, in partial fulfillment of the requirements for the degree of **MASTER OF SCIENCE IN MECHANICAL ENGINEERING DEPARTMENT**.

Thesis Committee

Dr. Amro M. Al-Qutub (Adviser)

Dr. Mohamed A. Antar (Member)

Dr. Mostafa ElSharqawy (Member)

Dr. Zuhair M. Gasem
Department Chairman

Dr. Salam A. Zummo
Dean of Graduate Studies

29/5/14
Date

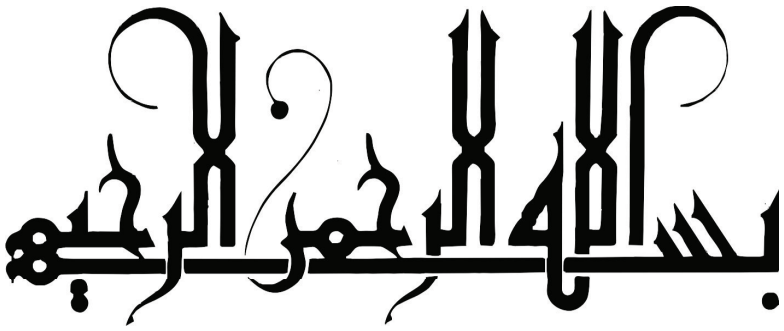

DEDICATED TO

my beloved parents

Mohammad Ali Almunteshari

&

Abdeleya Obaidallah Almunteshari

my brother

Abdullah

my wife

Amal Ahmad Almunteshari

my little daughter

Layan

ACKNOWLEDGMENTS

In the name of Allah, the most Compassionate, the most Merciful. I am most grateful to Allah for He bequeaths me the favor to live in sound health and to undertake this task successfully.

I am thankful to the authority of the King Fahd University of Petroleum and Minerals, especially the Mechanical Engineering Department for providing me the environment to pursue this level of study. I am also thankful to the Clean Water Clean Energy Center (KFUPM-MIT collaboration) for giving me the opportunity to conduct two months of research at MIT. I wish to appreciate the kindness and encouragement of my thesis committee, comprised of Dr. Amro Alqutob, Dr. Mohammad Antar and Dr. Mostafa Elsharqawy. Without their high quality advice, encouragement and good human relationship, this work may not have come to fruition. I am proud to have you as my committee members. I am particularly thankful to my advisor, Prof. Amro Alqutub for his patience in spite of all my shortcomings. I must confess that this work attained the status of a Master thesis due to his untiring attitude to encouraging, advising and supporting me throughout the course of this work.

I am also grateful to Dr. Fahad Alsulaiman and Dr. Syed Zubair who were very helpful and supportive. I appreciate the assistance of Eng. Bha'a Aldeen (Abo

Ahmad) from Mechanical Engineering Department for his practical assistance and support throughout the work. My gratitude goes to all Mechanical Engineering graduate students, faculty and staff.

I am highly indebted in thanks to my entire family members. Your kind physical, moral and spiritual supports have been my source of propulsion to achieving any worthy endeavors. I am proud of you all.

To all my friends and colleagues, I am ever grateful to you all. I can not imagine what this experience would be have been without your supports. Thank you all.

TABLE OF CONTENTS

LIST OF TABLES

LIST OF FIGURES

Nomenclature

Acronyms

GOR	Gained-Output-Ratio
HCR	Heat Capacity Rate Ratio
HDH	Humidification Dehumidification
SHI	Specific Heat Input
TDMC	Thermal Driven Mechanical Compression
VPR	Vapor Productivity Ratio

Roman Symbols

A	area [cm^2]
C_d	discharge coefficient [-]
D	column diameter [mm]
d	orifice plate diameter [mm]
g	gravitational acceleration [m/s^2]
$\dot{H}$	total enthalpy rate [W]

h	specific enthalpy [J/kg]
h_{fg}	specific enthalpy of vaporization [J/kg]
K	pressure losses coefficient [-]
$\dot{m}$	mass flow rate [kg/s]
$\dot{m}_r$	mass flow rate ratio [kg/s]
P	pressure [kPa]
Pr	pressure ratio [-]
$\dot{Q}$	heat transfer rate [W]
Re	Reynolds number [-]
Re_j	Reynolds number through the jet [-]
s	specific entropy [J/kg.K]
V_j	air jet velocity [m/s]
$\dot{\forall}$	volumetric flow rate [cm^3/s]
V_{SG}	air superficial velocity [cm/s]
$\dot{W}$	work transfer rate [W]
z	differential head in manometer [cm]

Greek Symbols

β	diameter ratio d/D [-]
Δ	change or difference [-]
η	isentropic efficiency [-]

ε	energy effectiveness [-]
ω	specific humidity [kg_w/kg_a]
Ω	humidifier efficiency [-]
ϕ	relative humidity[-]
ρ	density [kg/m^3]

Superscript

ideal	ideal condition
ise	isentropic
sat	saturation

Subscript

a	air
c	compressor
cold	cold stream
D	dehumidifier
da	dry air
H	humidifier
hot	hot stream
HX	heat exchanger
i	inlet
in	entering

max	maximum
o	outlet
out	leaving
pw	product water
t	turbine
w	water
wb	wet bulb

THESIS ABSTRACT

NAME:	Obaidallah Mohammad Ali Munteshari
TITLE OF STUDY:	Multi-stage Bubble Column Humidifier for Thermal Driven Mechanical Compression Humidification Dehumidification Desalination System
MAJOR FIELD:	Mechanical Engineering Department
DATE OF DEGREE:	APRIL 2014

Humidification dehumidification (HDH) desalination systems have received significant attention due to their simplicity and dependence on low grade/renewable energy sources such as solar energy. These systems are suitable for low to medium scale water production for remote and off-grid areas. Among the many configurations of HDH desalination cycles is the varied-pressure HDH desalination cycle. This cycle can be driven mechanically using an external mechanical energy device such as a motor or a heat engine. A novel cycle is presented in this work in order to enhance the cycle performance. In the novel cycle, the carrier gas is heated before the expander to produce the work required to drive the compressor and to avoid using an external mechanical energy source. Then, thermodynamic analy-

sis is performed to understand effects of different key parameters. Based on the thermodynamic analysis of this cycle, it is essential to have a high humidifier's effectiveness to obtain high performance. Therefore, an experimental investigation on a multi-stage bubble column humidifier is presented. In the bubble column humidifier, air is blown into the column through a perforated plate located at the bottom of the column to form bubbles in a pool of hot water. The formation of bubbles increases the time and surface of contact, which results in an improvement in the humidification performance. In this work, effects of different parameters on the humidifier performance are studied. These parameters include air superficial velocity and mass flow rate ratio, water gate height and sparger profile.

THESIS ABSTRACT (ARABIC)

ملخص الرسالة

الاسم الكامل: عبيدالله محمد علي المنتشري

عنوان الرسالة: مرطب الهواء بالفقاعات متعدد الأدوار للعمل على نظام الترطيب والتكثيف لتحلية المياة الذي يعمل بالطاقة الحرارية ويضغط الهواء ميكانيكيا.

التخصص: هندسة ميكانيكية.

تاريخ الدرجة العلمية: جمادى الآخر 1435 هـ - ابريل 2014 م

تقنية الترطيب والتكثيف (humidification dehumidification) هي أحد التقنيات التي لقيت رواجاً كبيراً في الآونة الأخيرة، وذلك لبساطتها وإمكانية عملها على الطاقة الشمسية، كما أن هذه التقنية مناسبة للتطبيقات الصغيرة والمتوسطة، حيث أنه يسهل نقلها إلى الأماكن النائية. لهذه التقنية أنواع عديدة، من بين هذه الأنواع : الترطيب والتكثيف عند ضغوط مختلفة، حيث أن المرطب (humidifier) يعمل عند ضغط اقل من ضغط المكثف (dehumidifier). للمحافظة على فرق الضغط في هذا النظام لابد من مصدر خارجي لتشغيل الضاغط (compressor) كالمحرك أو المكينة الحرارية. في هذا البحث تم تطوير هذا النظام للاستغناء عن الحاجة إلى أي مصدر خارجي، وايضاً لرفع كفاءة النظام لذلك تم إضافة مسخن للهواء (heater) قبل دخول الهواء إلى محرك التربين (turbine) وذلك لتوفير الطاقة المطلوبة لجعل التوربين يشغل ضاغط الهواء حتى يتمكن من ضغط الهواء إلى الضغط المطلوب. يهدف هذا البحث لمعرفة مدى كفاءة هذا النظام حيث تم دراسة الديناميكية الحرارية لمعرفة تأثير أجزاء وعناصر النظام على أداءه. يعتبر المرطب (humidifier) أحد أهم أجزاء هذا النظام ومن أكثرها تأثيراً على أداء النظام ، ولهذا فإن الهدف الثاني لهذه الرسالة هي تطوير مرطب الفقاعات متعدد الأدوار (multi-stage bubble column humidifier) ودراسة هذا المرطب معملياً للحصول على أعلى كفاءة ممكنة مع خسارة قليلة نسبياً في الضغط.

CHAPTER 1

INTRODUCTION

1.1 Motivation

The need for fresh water is dramatically increasing with the increase in population growth and unsustainable consumption rate. Many countries face a huge water scarcity as shown in Figure 1.1. The sacricity of the fresh water is expected to be the biggest issue in the 21^{st} century. So, the use of desalination systems is essential to solve this issue. Many conventional desalination technologies are being used around the world such as multiple effect desalination (MED), multi-stage flash (MSF) and reveres osmosis (RO) [1] . However, these technologies are usually on a large scale and most suitable for economically advanced and rich in energy resources regions of the world. Most of the developing countries which are suffering from water scarcity do not have sufficient energy resources to run these technologies. Moreover, delivering distilled water to remote areas faces many difficulties. So, developing small-scale desalination technologies, which can

use solar energy, is an attractive solution, especially for poor and remote areas. Humidification dehumidification desalination system (HDH) [2], which mimics the water (rain) cycle in nature, is a promising technology to resolve this issue.

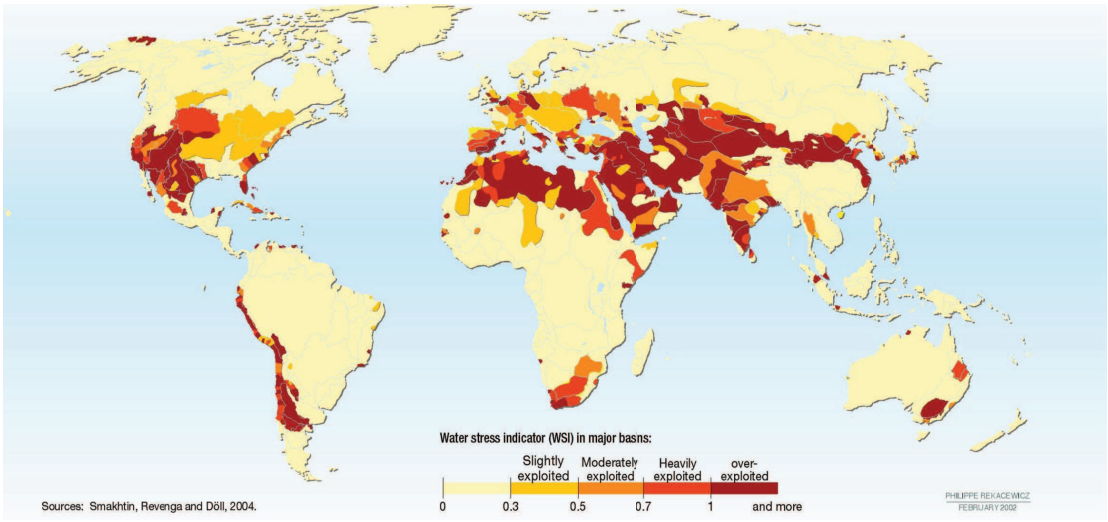

Figure. 1.1: Water scarcity index [3].

1.2 Varied-pressure humidification dehumidification desalination system review

HDH has recently received considerable attention. The simplest cycle is illustrated in Figure 1.2. The carrier gas, usually air, is humidified and heated simultaneously in the humidifier by direct contact with saline water. Then, the pure water is produced by condensing the humidified air in the dehumidifier.

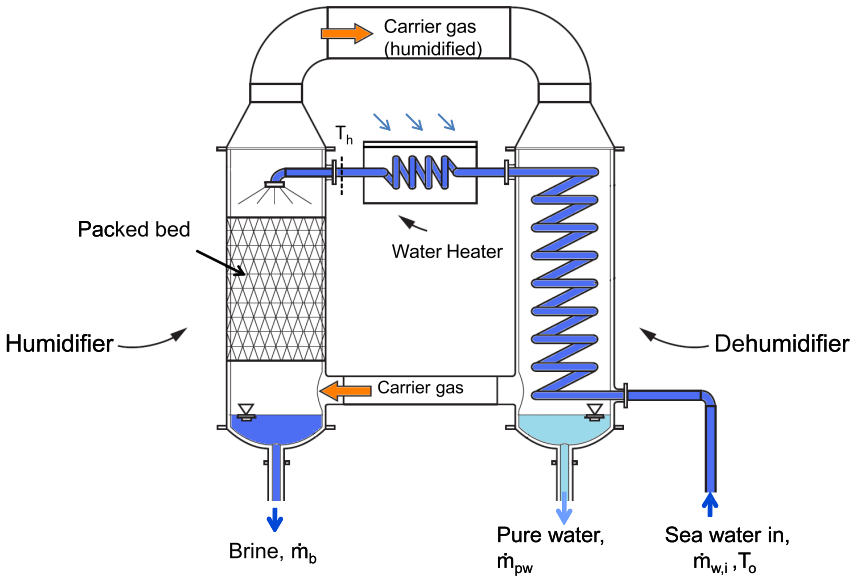

Figure. 1.2: Basic humidification dehumidification Cycle [2].

Among the many configurations of HDH desalination cycles presented in Figure 1.3 is the basic varied-pressure HDH desalination cycle as shown in Figure 1.4 [4]. This cycle includes four main items (a) Humidifier; (b) Dehumidifier; (c) Compressor; and (d) Expander. In this cycle, a carrier gas, mainly air, is humidified by saline water using a direct contact heat and mass exchanger device, called a humidifier. Then the carrier gas is compressed using a compressor in which both

pressure and temperature increase. An indirect contact dehumidifier is used to dehumidify the carrier gas and produce fresh water from the condensation of water vapor carried by the carrier gas. The carrier gas is then expanded in an expander that lowers the pressure and recovers some of the energy from the pressurized gas.

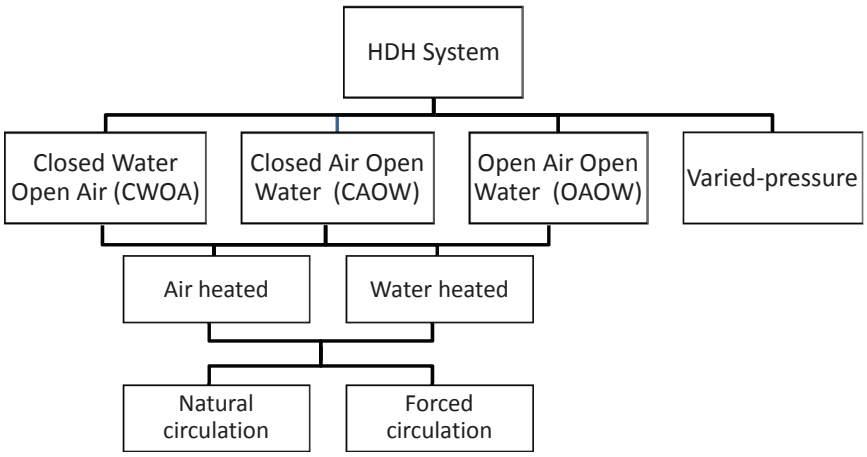

Figure. 1.3: HDH cycle configurations.

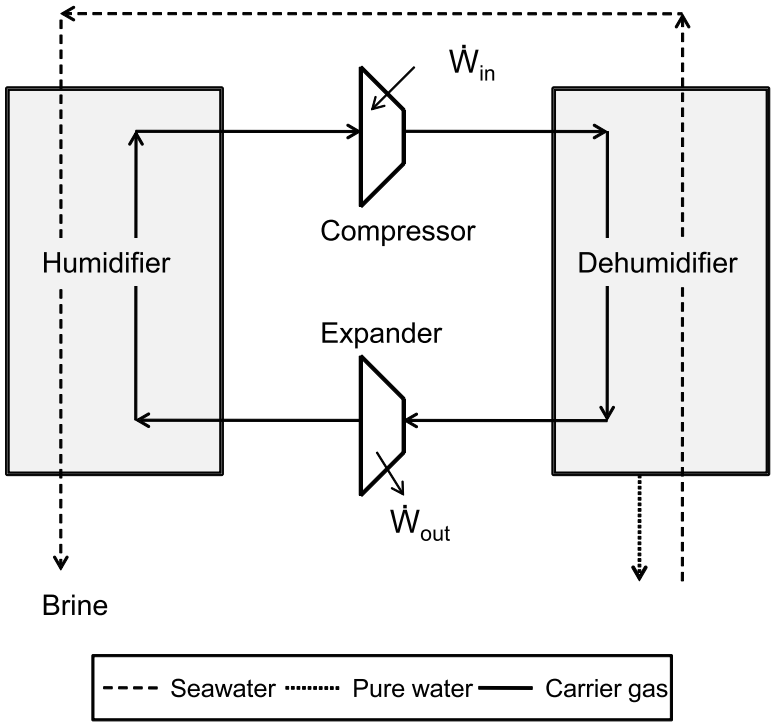

Figure. 1.4: Basic varied-pressure HDH [5].

Narayan et al. [4] studied the thermodynamic performance of different HDH systems. They found that the modified air-heated cycle shows a performance higher than the existing water-heated cycle. The humidifier and dehumidifier have similar effect on the performance of the modified air-heated cycle. Also, a varied pressure cycle is studied. It has high performance compared to the conventional HDH cycles.

Narayan et al. [5] performed more investigation on the varied-pressure HDH cycle. They analyzed the cycle in an on-design sense by defining the humidifier and dehumidifier effectivenesses and the compressor and expander isentropic efficiencies. This cycle has much higher performance compared to the conventional HDH cycles. However, it is less efficient than reverse osmosis and mechanical vapor compression since it consumes much more energy as shown in Table 1.1.

Table. 1.1: Comparison of mechanical compression HDH with other work driven small scale desalination technologies [5].

Technologies	**Energy consumed (kJ/kg)**
Reverse Osmosis (RO) with energy recovery	11-18
Mechanical vapor compression (MVC)	25-50
Mechanical compression HDH	200-260

Narayan et al. [6] studied a thermal vapor compression varied-pressure HDH cycle coupled with reverse osmosis unit. This cycle uses steam at high enthalpy with lower entropy rate which reduces the entropy generation in the system. The majority of the produced water came from the RO unit.

In the basic varied-pressure HDH cycle (Figure 1.4), the recovered work by

the turbine is much less than the consumed work by the compressor and this can be illustrated on the psychometric chart in Figure 1.5.

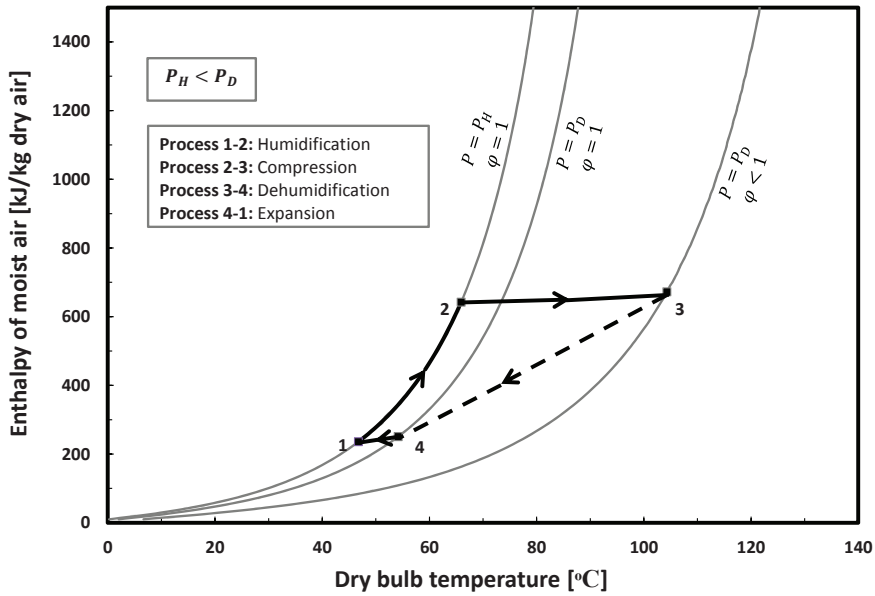

Figure. 1.5: Varied-pressure HDH cycle represented in psychometric chart

Thus, an external source of work besides the recovered work by the turbine is needed to run the compressor. One way of enhancing the recovered work is by coupling the turbine or compressor with a motor but this is not easily achievable. A sophisticated balance is imperative to couple the motor with the turbine or compressor which increases the cost of the cycle. Also, this will decrease the GOR of the cycle, since the GOR of the cycle is inversely proportional to the net work or heat input. Moreover, it is not possible to recover a work from a latent heat (condensation across the expander) since the expander deals with sensible heat only. So, more research and development need to be done to improve the varied-pressure HDH cycle.

1.3 Bubble column humidifier review

Heat and mass transfer devices (humidifier and dehumidifier) play a key role in the HDH systems. In the humidifier of a humidification dehumidification system, heat and mass simultaneously transfer from the water stream, which comes from the dehumidifier or heater, to the air stream that comes from the ambient. There are several devices that could be used as a humidifier for the HDH systems. These devices include packed bed towers, spray towers, wetted-wall towers, and bubble columns [7].

In the spray tower, water is sprayed at the top of a cylindrical column and falls in the form of droplets due to gravity while a running air stream flows upward to be in direct contact with the water droplets as shown in Figure 1.6. Mist eliminators are essential to avoid water entrainment in the air leaving the column. These types of humidification devices have low effectiveness due to the low water hold-up. Moreover, the pressure drop in the water stream is high due to the losses in the spray nozzles [8].

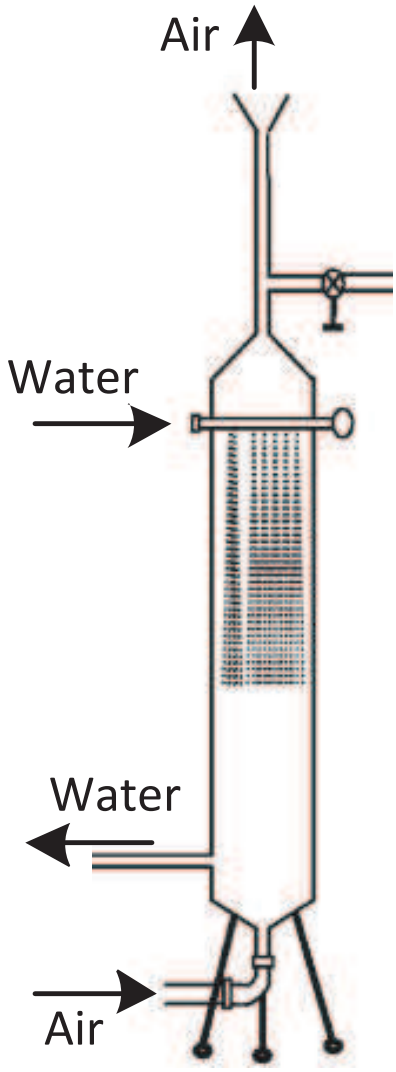

Figure. 1.6: spray tower [9].

Wetted-wall towers could be used as a humidification chamber in the HDH system. The wetted-wall tower is operated by running a thin film of water downward on the inner perimeter of the column to form a wet surface along the column length while an air stream flows, either upward or downward, in the column as shown in Figure 1.7. Air side pressure drop in these devices is probably lower than the other humidification towers [8]. In addition, it shows high humidification efficiency [10]. However, this device has low water flow rate capacity since

the water only flows on the inner surface of the tower.

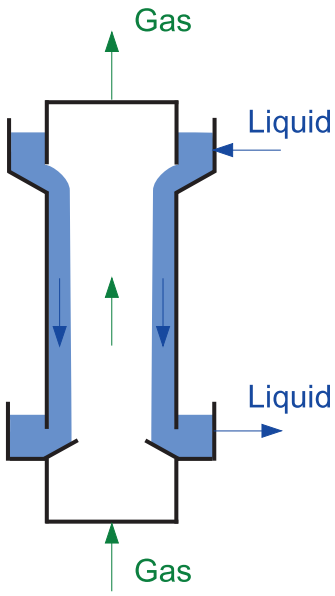

Figure. 1.7: Wetted-wall tower.

The packed bed tower is widely used as a humidifier in the HDH system [11–15]. It is similar to the spray tower in using spray nozzles. However, in the packed bed towers as shown in Figure 1.8, the column is filled with packing material to enhance the humidification efficiency since the water droplets are more dispersed in this packing material, which increases the contact time and contact surface.

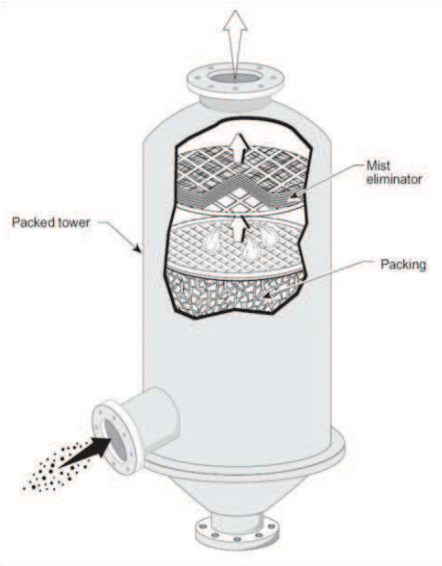

Figure. 1.8: Packed bed tower [16].

Recently, the bubble columns have received much consideration and has been highlighted as a good replacement for packed bed towers [17]. In the bubble column humidifier, hot water enters the bubble column and accumulates till it reaches a certain level while air is injected into the column through a perforated plate or perforated pipe (sparger) located at the bottom of the column to form bubbles in the pool of the hot water. Mass and heat transfer coefficients are maximized due to water diffusion into the air bubbles. This device is simple in design with low cost.

El-Agouz and Abugderah [18] investigated the performance of a single stage bubble column humidifier experimentally. An evaporator chamber with a square cross section of 500mm $\times$ 250mm and 700mm height has been used in their experiment. The air stream enters into the humidifier through 32 holes of 10mm diameter located on both sides of a 75mm diameter PVC pipe, which is submerged in a pool of water in the humidifier. They have studied the effect of different oper-

ational conditions including water level difference, water and air temperature and air flow rate on the vapor content difference and the bubble column humidifier efficiency. The obtained results showed that the performance of the bubble column is substantially affected by the air velocity and the inlet water temperature. The difference of vapor content was high compared to that obtained by Garg et al. [19] for the single stage packed bed tower and very similar to the multi-stage spray tower obtained by Chafik [20, 21] and Amara et al. [22]. Within the range of operational conditions studied, the maximum performance obtained for the humidifier was 95% of humidification efficiency with $222 g_w/kg_a$ of vapor content difference at $75°C$ for air and water.

Another study by El-Agouz [23] has been performed using a single stage bubble column humidifier with a square cross section of 400mm $\times$ 300mm and 1000mm height. Air stream enters into the humidifier through 44 holes of 15mm diameter located on the top side of a 75mm diameter copper pipe, which is submerged in a pool of brackish water in the humidifier. The experimental work studied the influence of different operational conditions on the desalination performance. These operational conditions include the water level in the column, the water temperature, and the air flow rate. The obtained results showed that the humidification efficiency is slightly affected by the water level whereas it is strongly affected by the air flow rate and water temperature. As the air flow rate and water temperature increase, the humidification efficiency increases. The maximum humidification efficiency obtained is 98% at $85°C$ of brackish water temperature

and 14 kg/hr of air flow rate.

Zhang et al. [24] have conducted an experiment on the influence of the water level and air flow rate on the air relative humidity and the pressure drop in a single stage bubble column humidifier. The humidifier is constructed from a sieve plate of 198mm diameter and 8mm thickness, used as a sparger. The sieve plate contains 91 holes of 1mm diameter which are distributed in the form of an equilateral triangle with an interval of 18mm. The obtained results showed that the air relative humidity reached 100%. Although the experiment was performed at a low air superficial velocity (less than 2.3cm/s), the pressure drop exceeded 2 kPa where air superficial velocity is defined as the ratio of the volumetric flow rate to the cross sectional area of the bubble column.

Recently, Narayan et al. [25] used the bubble column as a dehumidifier. They investigated cooling and condensing the moist air in a column of cold water rather than on a cold surface. In this study, under the same operational conditions, a maximum heat flux of 8 kW/m^2 was obtained in the bubble column dehumidifier compared to a maximum heat flux of 1.8 kW/m^2 which could be obtained using a typical dehumidifier produced from George Fischer LLC.

Table 1.2 presents a summary of the literature for bubble column humidifier investigations.

Table. 1.2: Summery of the literature review

Author(s)	**Sparger**			**Column**	**Studied Parameters**	**Operational conditions**	**Max. output**
	# of holes	Holes diameter	Sparger shape				
El-Agouz and Abugderah [18]	32	10 mm	Holes on both side of 75 mm PVC Pipe	500 mm × 250 mm square cross section	Ω , $\Delta\omega$	30°C $<$ T_w $<$ 75°C 30°C $<$ T_a $<$ 75°C 8.8 cm/s $<$ V_{SG} $<$ 26 cm/s 1.7 cm $<$ ΔH $<$ 7 cm	Ω_{max} = 95% $\Delta\omega_{max}$ = 222 g_w/kg_a
El-Agouz [23]	44	15 mm	Holes on upper side of 75 mm copper pipe	400 mm × 300 mm square cross section	Ω , $\Delta\omega$	40°C $<$ T_w $<$ 85°C 0.8 cm/s $<$ V_{SG} $<$ 2.7 cm/s 20 cm $<$ H $<$ 60 cm	Ω_{max} = 98% $\Delta\omega_{max}$ = 800 g_w/kg_a
Zhang et al. [24]	91	1 mm	Perforated plate	cylindrical chamber of 198 mm diameter	ΔP, ϕ	30°C $<$ T_w $<$ 80°C 30°C $<$ T_a $<$ 80°C 0.4 cm/s $<$ V_{SG} $<$ 2.3 cm/s 6 cm $<$ H $<$ 18 cm	ΔP is too high ϕ_{max} = 100%

The following equation was used in the previous publications [10, 18, 21, 23] in order to evaluate the bubble column humidifier efficiency.

$$\Omega = \frac{\omega_{out} - \omega_{in}}{\omega_{out}^{sat} - \omega_{in}} \tag{1.1}$$

where ω_{in} and ω_{out} are the inlet and outlet specific humidity of the humidifier and ω_{out}^{sat} is the outlet specific humidity at saturation. This definition is not appropriate to evaluate the performance of the humidifier since ω_{out}^{sat} is evaluated at the exit air temperature without any consideration of water temperature. So, a new definition is needed to evaluate the performance of the humidifier correctly. Narayan et al. [26] proved that an energy based effectiveness definition is the most appropriate definition for evaluating the humidifier effectiveness.

1.4 Objectives

This thesis attempts to address the following matters:

1. Developing the basic varied-pressure HDH cycle and, then, studying the thermodynamic performance analysis of the new cycle called Thermal Driven Mechanical Compression HDH cycle (TDMC-HDH). In order to optimize the design of the new cycle, it is necessary to understand the effect of key parameters on the overall performance of the system (GOR). These parameters include effectivenesses of the components, compressor pressure ratio, temperature and relative humidity of the inlet air, temperature of water entering the cycle and air side pressure losses in the system's components. This analysis is performed in Chapter 2.

2. Designing and evaluating experimentally a novel system of multi-stage bubble column humidifier in order to achieve high effectiveness with acceptable pressure losses. The evaluated parameters include air superficial velocity, mass flow rate ratio, water gate height and sparger profile. Then, results of the multi-stage bubble column humidifier are incorporated with the new HDH cycle model to evaluate the performance. This is performed in Chapter 3.

CHAPTER 2

THERMODYNAMIC ANALYSIS OF TDMC-HDH CYCLE

2.1 Thermal driven mechanical compression HDH cycle

In this chapter, a novel varied-pressure HDH cycle is proposed. The new cycle called thermal driven mechanical compression humidification dehumidification desalination system (TDMC-HDH) operates the humidifier and dehumidifier chambers at different pressures. Figure 2.1 shows the main components of the modified cycle; including (a) humidifier, (b) dehumidifier, (c) heat exchanger, (d) heater and (e) turbocharger (compressor and turbine). The difference in the pressure is maintained using the compressor and the turbine coupled together by a shaft (tur-

bocharger). The air is operated in an open loop where it is heated and humidified in the humidifier. Then, the humidified air is compressed using the compressor and then cooled and condensed in the dehumidifier. Thereafter, the dehumidified air is heated by the recovered heat from the turbine's exhaust. However this heat is not enough to achieve the temperature required by the turbine to run the compressor. So, more heat is added using an external source. Afterward, the air expands in the turbine to recover energy in the form of a work transfer.

In the water cycle, the water is heated in the dehumidifier by recovering some of the thermal energy gained by the air in the compression process. After that, the water goes to the humidifier to heat and humidify the air. The brine from the humidifier is then disposed of while the distilled water is collected from the dehumidifier.

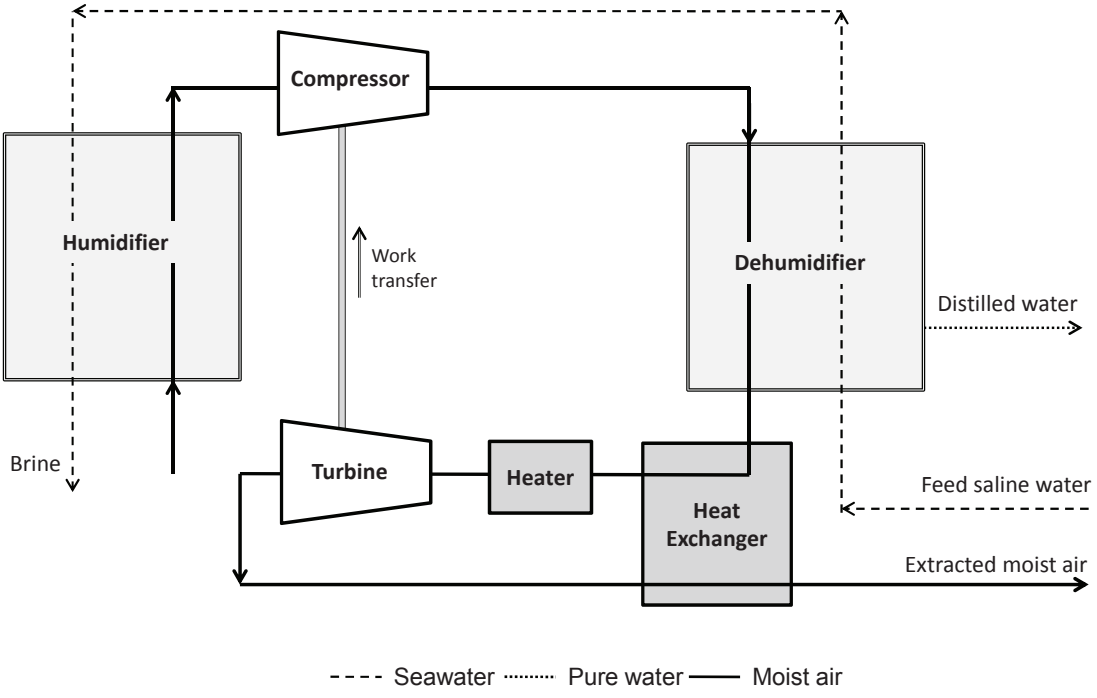

Figure. 2.1: Thermal driven mechanical compression HDH cycle

2.2 System and performance parameters

The parameters used to evaluate the performance of the HDH cycle are presented in this section. These parameters include Gained-Output-Ratio (GOR), vapor productivity ratio (VPR), specific heat input (SHI), energy effectiveness (ε) and heat capacity rate ratio (HCR).

2.2.1 Gained-Output-Ratio

GOR is a common parameter to measure the performance of a thermal desalination plant. It is defined as the ratio of the enthalpy of vaporization of the produced water to the heat input to the system.

$$\text{GOR} = \frac{\dot{m}_{pw} h_{fg}}{\dot{Q}_{in}} \tag{2.1}$$

Also, GOR is a function of two system parameters. These parameter are vapor productivity ratio (VPR) and specific heat input (SHI).

$$\text{GOR} = \underbrace{\left\{\frac{\dot{m}_{pw}}{\dot{m}_{da}.\omega_{H,o}}\right\}}_{\text{VPR}} \cdot \underbrace{\left\{\frac{\dot{m}_{da}.\omega_{H,o}}{\dot{Q}_{in}}\right\}}_{1/\text{SHI}} \cdot \underbrace{\{h_{fg}\}}_{\text{almost constant}} \tag{2.2}$$

Enthalpy of vaporization (h_{fg}) in these equations is calculated at the temperature of the water entering the dehumidifier.

2.2.2 Vapor productivity ratio (VPR)

VPR is defined as the ratio of the produced water rate ($\dot{m}_{pw}$) to the rate of compressed water vapor (at the humidifier exit) ($\dot{m}_{da}.\omega_{H,o}$) in the system .

$$\text{VPR} = \frac{\dot{m}_{pw}}{\dot{m}_{da}.\omega_{H,o}} \tag{2.3}$$

VPR is an indicator for humidifier and dehumidifier effectivenesses. Since the water produced can not be more than the compressed water vapor, the value of VPR is always less than unity. High value of VPR is preferred which means more compressed water vapor is condensed in the dehumidifier.

2.2.3 Sapicific heat input (SHI)

SHI is defined as the ratio of the heat input to the system ($\dot{Q}_{in}$) to the rate of compressed water vapor (at the humidifier exit) ($\dot{m}_{da}.\omega_{H,o}$).

$$\text{SHI} = \frac{\dot{Q}_{in}}{\dot{m}_{da}.\omega_{H,o}} \tag{2.4}$$

The amount of heat input depends on the rate of compressed water vapor since this heat is utilized by the turbine to provide the work needed by the compressor. Low value of SHI means that less heat needed to compress the moist air exiting from the humidifer.

2.2.4 Energy effectiveness

The energy effectiveness for adiabatic heat and mass exchange devices is defined as the ratio of total enthalpy rate difference ($\Delta\dot{H}$) to the maximum possible total enthalpy rate difference ($\Delta\dot{H}_{max}$). Depending on which stream has the maximum heat capacity rate, the maximum possible change in total enthalpy rate can be of either the moist air or water stream. Further discussion of this concept can be found in the work of Narayan et al. [26].

$$\varepsilon = \frac{\Delta\dot{H}}{\Delta\dot{H}_{max}} \tag{2.5}$$

2.2.5 Heat capacity rate ratio

In this work, the heat capacity rate ratio for the heat and mass exchange devices is defined as the ratio of the maximum possible change in the total enthalpy rate of the cold stream to the maximum possible change in the enthalpy rate of the hot stream. The theory behind this definition is explained by Narayan et al. [27].

$$\text{HCR} = \frac{\Delta\dot{H}_{max,cold}}{\Delta\dot{H}_{max,hot}} \tag{2.6}$$

It was shown that the entropy generation of a heat and mass exchange device is minimized when the heat capacity ratio is equal to unity, irrespective of the values of other variables [27].

2.3 Equations and modeling details

In order to evaluate the performance of the thermal driven mechanical compression humidification dehumidification desalination systems, a thermodynamic analysis has been performed. The following approximations and assumptions have been made to achieve the thermodynamic analysis [4]:

1. The processes work at steady-state conditions.
2. Heat losses from the system components to the ambient are neglected.
3. Power of the pump is negligible compared to the input heat.
4. In the energy balance equation, the potential and kinetic terms are neglected.
5. The distilled water leaves the dehumidifier at the average temperature of the moist air dew point at the inlet of the dehumidifier and the moist air dry bulb at the outlet of the dehumidifier.
6. Mechanical losses in the turbocharger are neglected.

Figure 2.2 shows stations' numbering where the processes between the stations are described in Table 2.1.

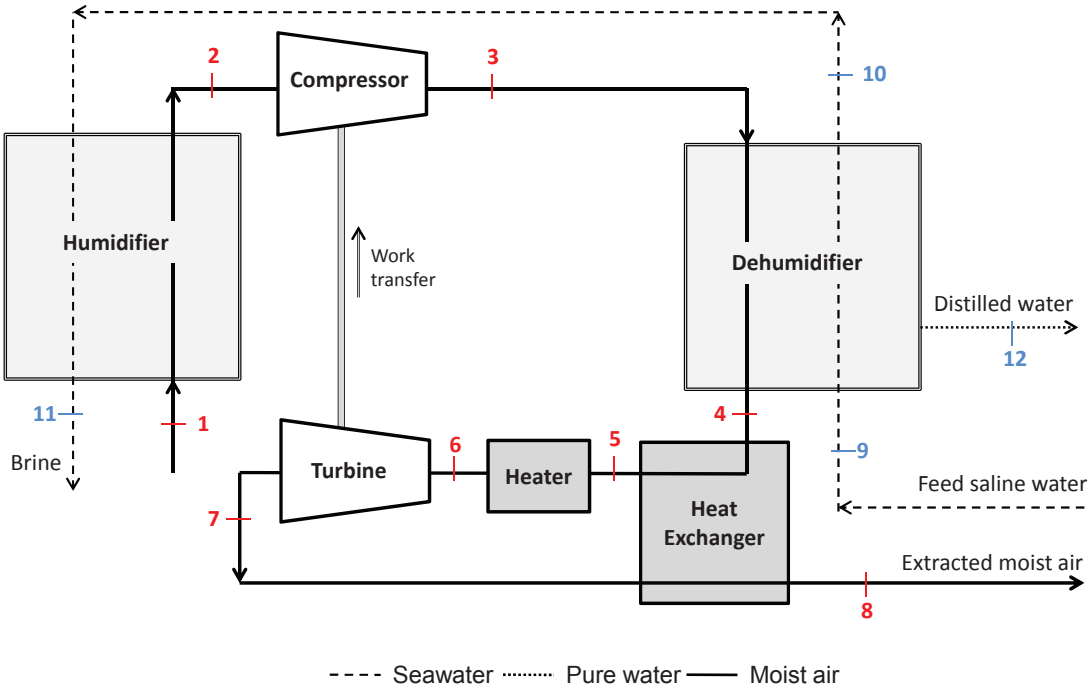

Figure. 2.2: Thermal driven mechanical compression HDH cycle stations

Table. 2.1: Processes of TDMC-HDH cycle

Station	Component	Process
$1 \rightarrow 2$ & $10 \rightarrow 11$	Humidifier	humidification
$2 \rightarrow 3$	Compressor	compression
$3 \rightarrow 4$ & $9 \rightarrow 10$	Dehumidifier	dehumidification
$4 \rightarrow 5$ & $7 \rightarrow 8$	Heat exchanger	recovering heat
$5 \rightarrow 6$	Heater (Burner)	heating
$6 \rightarrow 7$	Turbine	expansion

2.3.1 Humidifier

There are two counter-flow streams in the humidifier. One stream is the water that comes from the dehumidifier and the other stream is the air that comes from ambient. Based on the mass conservation principle, the mass flow rate of dry air is constant through the system.

$$\begin{aligned} \dot{m}_{da} &= \dot{m}_{da,i} = \dot{m}_{da,o} \\ \Rightarrow \qquad &= \dot{m}_1 = \dot{m}_2 \end{aligned} \tag{2.7}$$

In the humidifier, the water stream is transferring mass and heat to the moist air. The mass balance equation across the humidifier is described by the following equation:

$$\begin{aligned} \dot{m}_{w,o} &= \dot{m}_{w,i} - \dot{m}_{da}(\omega_{a,o} - \omega_{a,i}) \\ \Rightarrow \quad \dot{m}_{11} &= \dot{m}_{10} - \dot{m}_{da}(\omega_2 - \omega_1) \end{aligned} \tag{2.8}$$

Based on the definition mentioned in Section 2.2.4, the energy effectiveness of the humidifier can be described in terms of mass flow rates and enthalpies by one of the following two equations:

Case I, $\Delta\dot{H}_{max,w} < \Delta\dot{H}_{max,a}$:

$$\begin{aligned} \varepsilon_H &= \frac{\dot{m}_{w,i}h_{w,i} - \dot{m}_{w,o}h_{w,o}}{\dot{m}_{w,i}h_{w,i} - \dot{m}_{w,o}h_{w,o}^{ideal}} \\ \Rightarrow \qquad &= \frac{\dot{m}_{10}h_{10} - \dot{m}_{11}h_{11}}{\dot{m}_{10}h_{10} - \dot{m}_{11}h_{11}^{ideal}} \end{aligned} \tag{2.9}$$

Case II, $\Delta\dot{H}_{max,w} > \Delta\dot{H}_{max,a}$:

$$\begin{aligned} \varepsilon_H &= \frac{h_{a,o} - h_{a,i}}{h_{a,o}^{ideal} - h_{a,i}} \\ \Rightarrow \qquad &= \frac{h_2 - h_1}{h_2^{ideal} - h_1} \end{aligned} \tag{2.10}$$

where h_{11}^{ideal} and h_2^{ideal} are calculated at the inlet air wet bulb temperature ($T_{wb,1}$) and inlet water temperature (T_{10}), respectively.

Based on the First Law of Thermodynamics, the energy balance of the humidifier is written as:

$$\begin{aligned} &\underbrace{\dot{m}_{da}(h_{a,i} - h_{a,o})}_{\Delta\dot{H}_a} + \underbrace{\dot{m}_{w,i}h_{w,i} - \dot{m}_{w,o}h_{w,o}}_{\Delta\dot{H}_w} = 0 \\ \Rightarrow \quad &\dot{m}_{da}(h_1 - h_2) + (\dot{m}_{10}h_{10} - \dot{m}_{11}h_{11}) = 0 \end{aligned} \tag{2.11}$$

where $\Delta\dot{H}_a$ represents the difference in the total enthalpy rate for the humid air stream and $\Delta\dot{H}_w$ represents the difference in the total enthalpy rate for the water stream.

2.3.2 Dehumidifier

Two counter-flow streams are considered in the dehumidifier. One stream is the feed water and the other is the humid air. In the dehumidification process, heat transfer from the humid air to the feed water causes condensation for some of the water vapor which forms distilled water.

Since there is no mass transfer from or to the feed water stream, its mass flow rate enters and leaves the dehumidifier at the same rate:

$$\begin{aligned} \dot{m}_{w,o} &= \dot{m}_{w,i} \\ \Rightarrow \quad \dot{m}_{10} &= \dot{m}_9 \end{aligned} \tag{2.12}$$

Using the mass balance across the dehumidifier, the flow rate of the condensed water can be calculated as following:

$$\begin{aligned} \dot{m}_{pw} &= \dot{m}_{da}(\omega_{a,i} - \omega_{a,o}) \\ \Rightarrow \quad \dot{m}_{12} &= \dot{m}_{da}(\omega_3 - \omega_4) \end{aligned} \tag{2.13}$$

The energy effectiveness of the dehumidifier is defined as follows:

Case I, $\Delta\dot{H}_{max,w} < \Delta\dot{H}_{max,a}$:

$$\begin{aligned} \varepsilon_D &= \frac{h_{w,i} - h_{w,o}}{h_{w,i} - h_{w,o}^{ideal}} \\ \Rightarrow \qquad &= \frac{h_9 - h_{10}}{h_9 - h_{10}^{ideal}} \end{aligned} \tag{2.14}$$

Case II, $\Delta\dot{H}_{max,w} > \Delta\dot{H}_{max,a}$:

$$\begin{aligned} \varepsilon_D &= \frac{\dot{m}_{da}(h_{a,o} - h_{a,i}) + \dot{m}_{pw}h_{pw}}{\dot{m}_{da}(h_{a,o}^{ideal} - h_{a,i}) + \dot{m}_{pw}h_{pw}} \\ \Rightarrow \qquad &= \frac{\dot{m}_{da}(h_4 - h_3) + \dot{m}_{12}h_{12}}{\dot{m}_{da}(h_4^{ideal} - h_3) + \dot{m}_{12}h_{12}} \end{aligned} \tag{2.15}$$

where h_{10}^{ideal} and h_4^{ideal} are evaluated at the inlet air temperature (T_3) and inlet water temperature (T_9), respectively.

Based on the First Law of Thermodynamics, the energy balance of the dehumidifier is written as:

$$\begin{aligned} &\underbrace{\dot{m}_{da}(h_{a,i} - h_{a,o}) - \dot{m}_{pw}h_{pw}}_{\Delta\dot{H}_a} + \underbrace{\dot{m}_{w,i}(h_{w,i} - h_{w,o})}_{\Delta\dot{H}_w} = 0 \\ \Rightarrow \quad &[\dot{m}_{da}(h_3 - h_4) - \dot{m}_{12}h_{12}] + \dot{m}_9(h_9 - h_{10}) = 0 \end{aligned} \tag{2.16}$$

where $\Delta\dot{H}_a$ represents the difference in the total enthalpy rate for the humid air stream and $\Delta\dot{H}_w$ represents the difference in the total enthalpy rate for the water stream.

2.3.3 Turbocharger

The turbocharger consists of a compressor and turbine coupled together by a shaft. The turbocharger is considered to be the heart of the thermal driven mechanical compression HDH cycle, since it maintains the pressure difference between the humidifier and the dehumidifier and recovers the work from the exhausted moist air and transfers it to the compressor.

$$\dot{W}_{out,t} = \dot{W}_{in,c} \tag{2.17}$$

Compressor

The compression work needed to maintain the pressure difference in the air stream is expressed as:

$$\begin{aligned} \dot{W}_{in,c} &= \dot{m}_{da}(h_{a,o} - h_{a,i}) \\ \Rightarrow \qquad &= \dot{m}_{da}(h_3 - h_2) \end{aligned} \tag{2.18}$$

The isentropic efficiency for the compressor is written as:

$$\begin{aligned} \eta_c &= \frac{h_{a,o}^{ise} - h_{a,i}}{h_{a,o} - h_{a,i}} \\ \Rightarrow \qquad &= \frac{h_3^{ise} - h_2}{h_3 - h_2} \end{aligned} \tag{2.19}$$

where, for the isentropic process, the state of the moist air at the exit of the

compressor is calculated using,

$$\begin{aligned} s_{a,o}^{ise} &= s_{a,i} \\ \Rightarrow \quad s_3^{ise} &= s_2 \end{aligned} \tag{2.20}$$

$$\begin{aligned} \omega_{a,o} &= \omega_{a,i} \\ \Rightarrow \quad \omega_3 &= \omega_2 \end{aligned} \tag{2.21}$$

Turbine (Expander)

The First Law of Thermodynamics for the turbine can be written as:

$$\begin{aligned} \dot{W}_{out,t} &= \dot{m}_{da}(h_{a,i} - h_{a,o}) \\ \Rightarrow \qquad &= \dot{m}_{da}(h_6 - h_7) \end{aligned} \tag{2.22}$$

The isentropic efficiency of the turbine is expressed as:

$$\begin{aligned} \eta_t &= \frac{h_{a,i} - h_{a,o}}{h_{a,i} - h_{a,o}^{ise}} \\ \Rightarrow \qquad &= \frac{h_6 - h_7}{h_6 - h_7^{ise}} \end{aligned} \tag{2.23}$$

where, for the isentropic process, the state of the moist air at the exit of the

turbine is calculated using,

$$\begin{aligned} s_{a,o}^{ise} &= s_{a,i} \\ \Rightarrow \quad s_7^{ise} &= s_6 \end{aligned} \tag{2.24}$$

$$\begin{aligned} \omega_{a,o} &= \omega_{a,i} \\ \Rightarrow \quad \omega_7 &= \omega_6 \end{aligned} \tag{2.25}$$

2.3.4 Heat Exchanger

Since the temperature of the moist air exhausted from the turbine is relatively high, a heat exchanger is added to recover some heat to the moist air stream before entering the heater. Based on the First Law of Thermodynamics, the heat exchanger energy balance can be expressed as:

$$\begin{aligned} \underbrace{h_{a,o} - h_{a,i}}_{\substack{\text{moist air stream coming} \\ \text{from the dehumidifier}}} &= \underbrace{h_{a,i} - h_{a,o}}_{\substack{\text{moist air stream coming} \\ \text{from the turbine}}} \\ \Rightarrow \qquad h_5 - h_4 &= h_7 - h_8 \end{aligned} \tag{2.26}$$

The effectiveness definition of the heat exchanger is as follows:

$$\begin{aligned} \varepsilon_{HX} &= \frac{h_{a,o} - h_{a,i}}{h_{a,o}^{ideal} - h_{a,i}} \\ \Rightarrow \qquad &= \frac{h_5 - h_4}{h^{7-h_4}} \end{aligned} \tag{2.27}$$

2.3.5 Heater

The temperature of the moist air at the exit of the dehumidifier is not high enough to drive the turbine even after recovering some heat in the heat exchanger. So, an external source of heat is added to reach to the temperature which turbine needs to run the compressor. The amount of heat added to the moist air stream can be calculated using the First Law of Thermodynamics,

$$\begin{aligned} \dot{Q}_{in} &= \dot{m}_{da}(h_{a,o} - h_{a,i}) \\ \Rightarrow \qquad &= \dot{m}_{da}(h_6 - h_5) \end{aligned} \tag{2.28}$$

2.4 Results and discussion

In this section, effects of various parameters on the overall performance of the system (GOR) are presented and discussed. Engineering Equation Solver (EES) [28] is used to solve the governing equations (Eqs. 2.1-2.28). In order to optimize the design of the cycle, it is necessary to understand the effect of the variation of key parameters. These parameters include: compressor pressure ratio; pressure losses; humidifier, dehumidifier and heat exchanger effectivenesses; and ambient conditions. The performance of the cycle is evaluated under the baseline values which are given in Table 2.2.

Table. 2.2: Baseline values

Parameter	Definition	Value	Unit
T_1	temperature of air entering the system	30	°C
T_9	temperature of water entering the system	25	°C
ϕ_1	relative humidity of air entering the system	50	%
P_H	humidifier pressure	101.3	kPa
$\dot{m}_{da}$	mass flow rate of dry air	0.1	kg/s
Pr	compressor pressure ratio	1.5	-
HCR_H	heat capacity rate ratio of the humidifier	1	-
ε_H	humidifier effectiveness	90	%
ε_D	dehumidifier effectiveness	90	%
ε_{HX}	heat exchanger effectiveness	85	%
η_c	compressor efficiency	78*	%
η_t	turbine efficiency	85	%
ΔP_H	pressure drop across the humidifier	0.5	kPa
ΔP_D	pressure drop across the dehumidifier	0.5	kPa
ΔP_{HX}	pressure drop across the heat exchanger	0.5	kPa

* Performance map of turbocharger used is illustrated in Appendix B.

In previous studies [4, 27], it was shown that the optimum performance occurs at HCR=1 for either the humidifier or dehumidifier. For mechanical compres-

sion varied-pressure HDH cycle, the overall entropy generation is minimized at a balanced condition of the humidifier ($\mathrm{HCR}_H = 1$) as illustrated in Figure 2.3 [5].

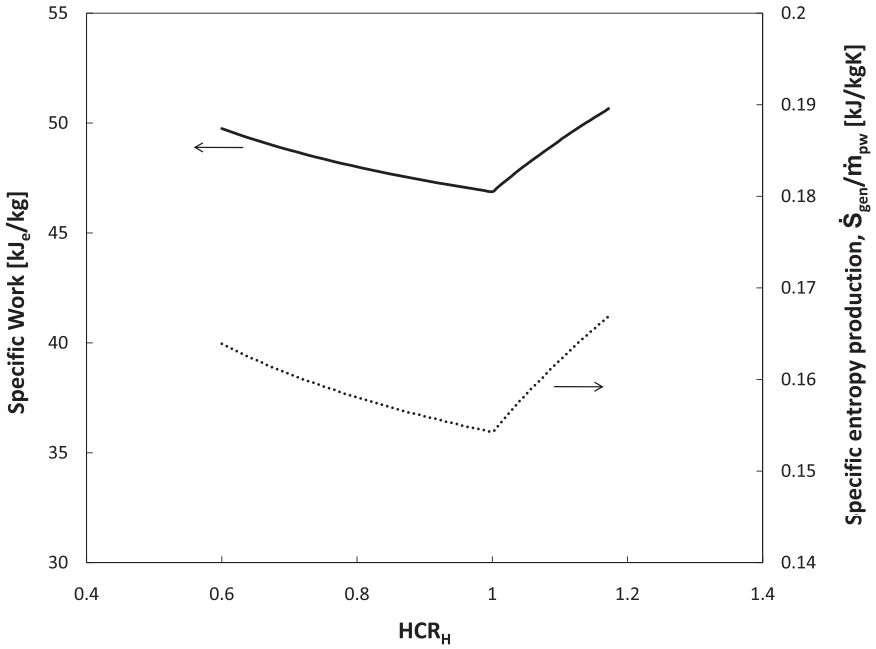

Figure. 2.3: Effect of heat capacity ratio of humidifier on specific work and specific entropy generation [5].

Figure 2.4 shows the variation of performance of the system (GOR) plotted against the heat capacity ratio of the humidifier for various values of water inlet temperature (T_9) at fixed values of humidifier and dehumidifier energy effectiveness, turbine and compressor efficiencies and the pressure ratio, as mentioned in Table 2.2. Irrespective of the value of water inlet temperature, GOR is maximized at $\mathrm{HCR}_H = 1$ whereas it is not the case for HCR_D since GOR is maximized at different values of HCR_D, as shown in Figure 2.5. Thus, the maximum GOR occurs at a balanced state for the humidifier. So, all the presented calculations are performed at $\mathrm{HCR}_H = 1$.

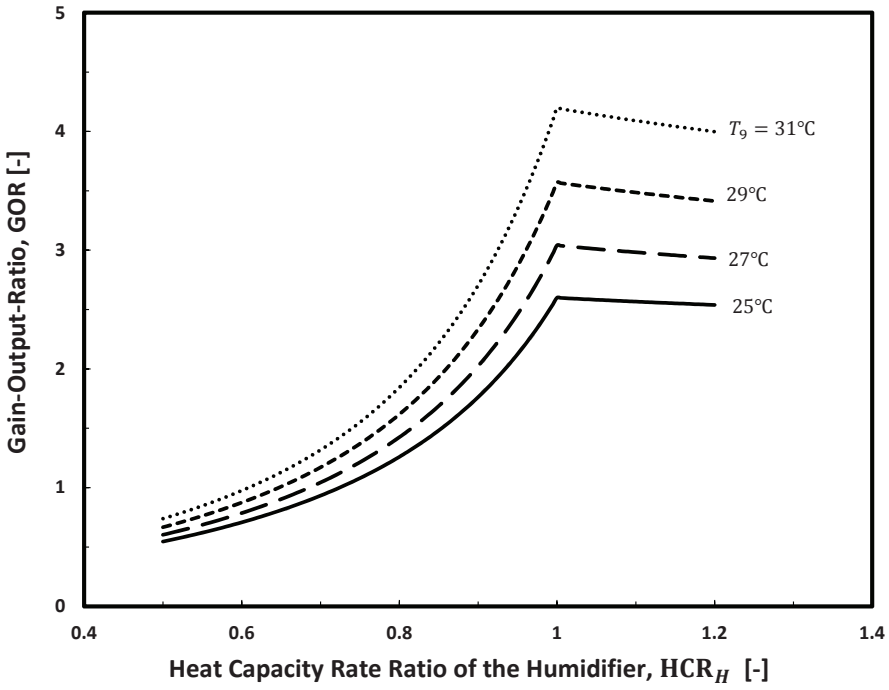

Figure. 2.4: HCR of the humidifier versus GOR for TDMC-HDH cycle at various water inlet temperatures.

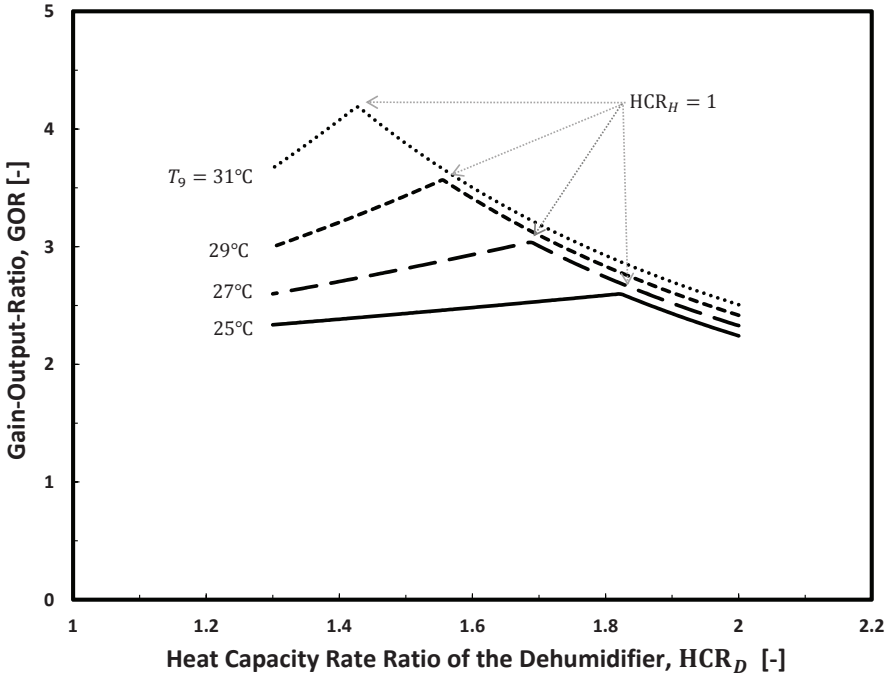

Figure. 2.5: HCR of the dehumidifier versus GOR for TDMC-HDH cycle at various water inlet temperatures.

2.4.1 Effect of pressure ratio and pressure losses

Pressure ratio, in this cycle, is expressed as the ratio of the pressure of the dehumidifier (P_D) to the pressure of the humidifier(P_H).

$$Pr = \frac{P_D}{P_H} \tag{2.29}$$

Pressure ratio and pressure losses are considered to be essential design parameters for the TDMC-HDH system since the system is operated at different pressures. Figure 2.6 illustrates the variation of GOR when the value of the pressure ratio is varied from 1.25 to 2. The effect of the pressure ratio is evaluated at 0, 1 and 2 kPa pressure losses in the system components ($\Delta P_H = \Delta P_D = \Delta P_{HX}$) while all other parameters are fixed at the baseline values shown in Table 2.2.

It is clear that at low pressure ratios the pressure losses cause a significant drop in the performance of the system. However, the effect of the pressure losses on the performance of the system diminises at high pressure ratio. So, operating the system at high pressure ratio is preferable to minimize the effect of the pressure losses. However, operating the system at very high pressure ratio will increase the cost and the size of the system and this needs to be optimized. Meanwhile, 1.5 pressure ratio is used to evaluate the effect of the other parameters.

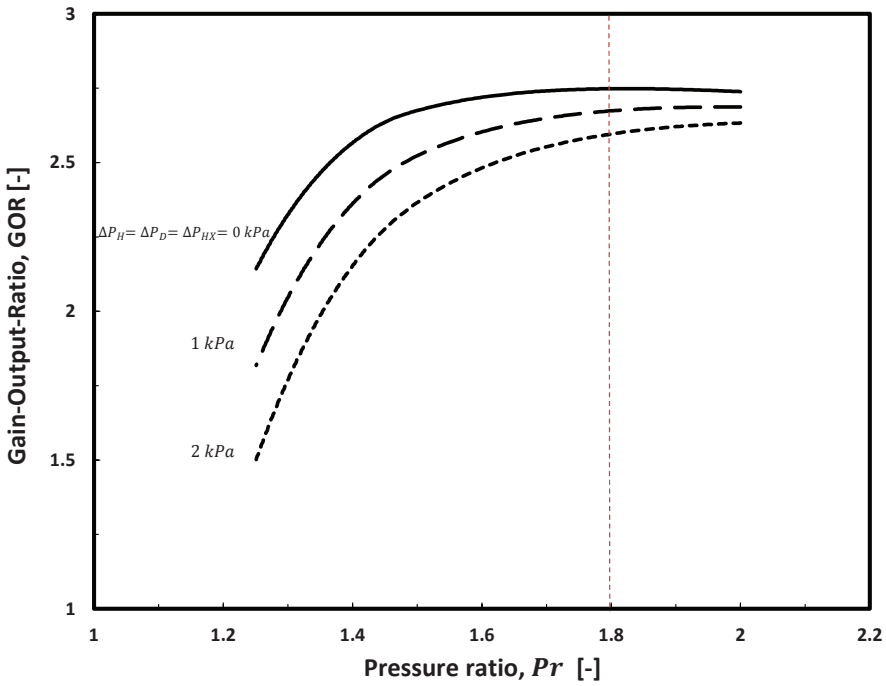

Figure. 2.6: Effect of pressure losses on performance of TDMC-HDH system.

Also, It is observed that the performance of the system (GOR) increases dramatically until it reaches $Pr = 1.8$ then slightly decreases. This variation in GOR can be explained by recalling the definition of GOR (Eq. 2.2) where GOR is a function of VPR and SHI. Figure 2.7 illustrates the variation of VPR and SHI against the pressure ratio. It is observed that VPR increases as Pr is increased. This trend is expected since the condensation process is enhanced by increasing the pressure in the dehumidifier side. SHI, on the other hand, is decreases dramatically till $Pr = 1.5$ then remains constant. High value of SHI because the performance of the compressor decreases at low pressure ratio (see Appendix B) which means more kilojoules of heat is needed to compress one kilogram of water vapor.

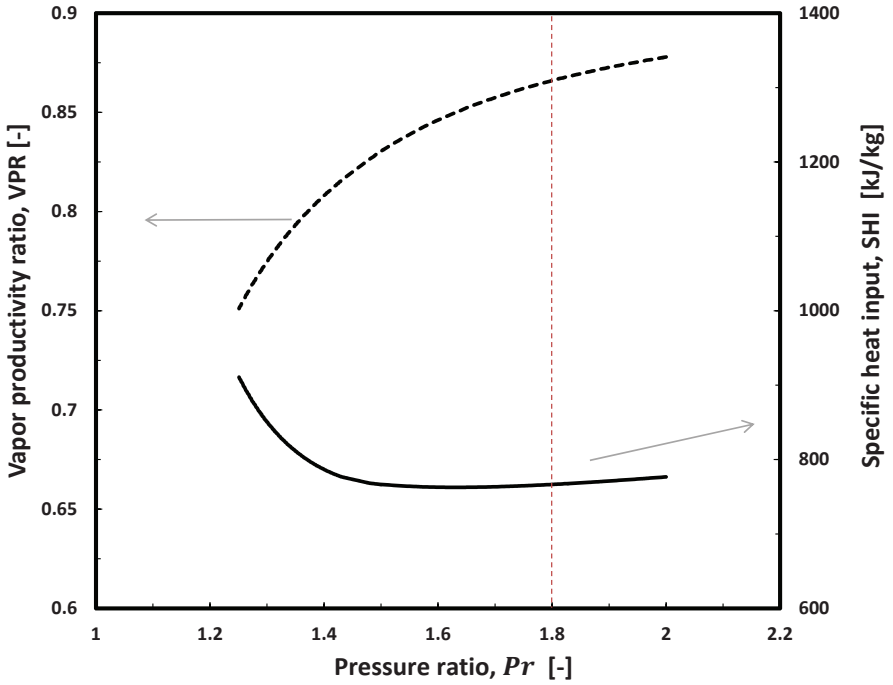

Figure. 2.7: The effect of pressure ration on vapor productivity ratio and rate of heat input.

2.4.2 Effect of humidifier, dehumidifier and heat exchanger effectivenesses

Figure 2.8 illustrates the effect of the components' effectivenesses on performance of TDMC-HDH cycle. In this figure, while one of the components' effectivenesses changes, the others are fixed at the baseline values. It is observed that GOR increases dramatically as components effectivenesses are increased. For example, if we increase the humidifier effectiveness from 80% to 90%, GOR will increase by 55%. In this cycle, both the humidifier and dehumidifier effectivenesses have a similar effect on the performance of the cycle. Therefore, developing humidifier and dehumidifier devices is essential to improve the performance of the system.

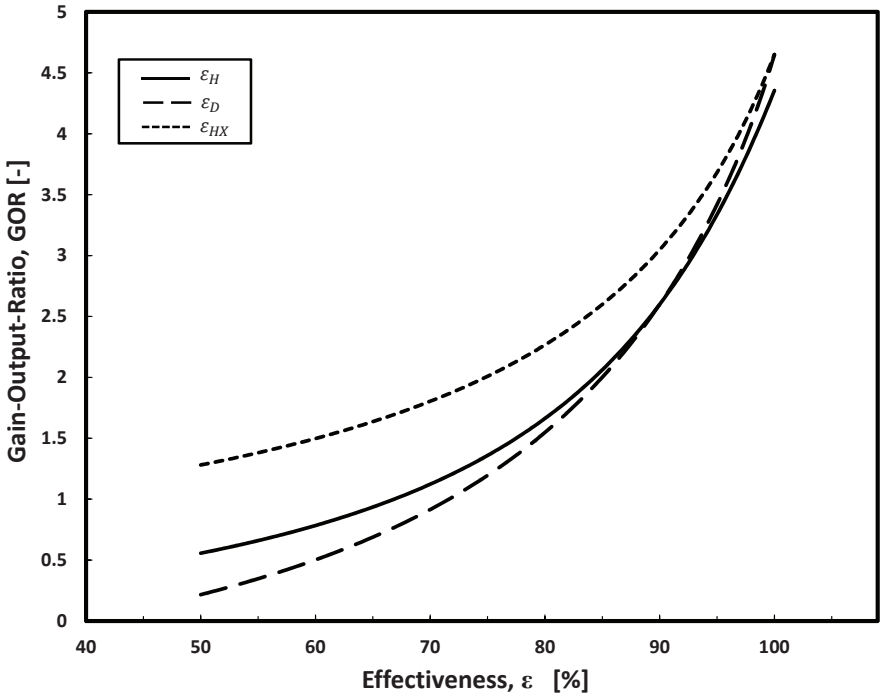

Figure. 2.8: Effect of humidifier, dehumidifier and heat exchanger effectivenesses on performance of TDMC-HDH system.

2.4.3 Effect of ambient conditions

This desalination unit is supposed to work outdoors where ambient conditions are changing continuously. So, studying the effect of ambient parameters that may affect the performance of the system is necessary. These parameters include the temperature and relative humidity of the air and the temperature of the water. Figure 2.9 shows the effect of air and water inlet temperatures on the performance of the system (GOR). The dashed lines represent the variation of air inlet temperature (entering the humidifier from the ambient) while the water inlet temperature is fixed at the given values. It is clear that GOR decreases as air inlet temperature increases. The reason behind this goes back to the configuration of the system where as the ambient temperature entering the humidifier increases,

the temperature of air entering the compressor increases. So, the compressor needs more work input to compress the air, which means more heat input. Therefore, the performance of the system (GOR) decreases.

The solid lines represent the effect of water inlet temperature (entering the dehumidifier from the ambient) variation on GOR while the air inlet temperature is fixed at the given values. The trend of the performance is expected since as the temperature of the water entering the dehumidifier increases, the temperature of the air exiting from the dehumidifier increases. Thus, a lower amount of heat will be added to the system which results in high performance (GOR).

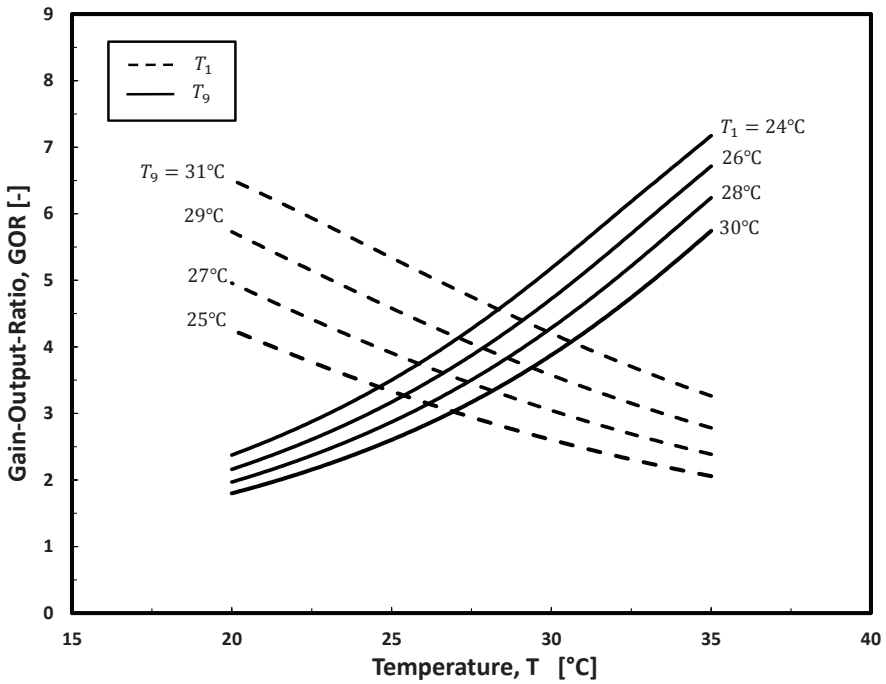

Figure. 2.9: Effect of the temperature of air and water entering the system from ambient on the performance of the system.

Figure 2.10 shows the effect of the air inlet relative humidity on the performance of the system (GOR) at various values of inlet air temperature. It is clear that GOR decreases with increasing inlet air relative humidity. This result may

seem contradicted with results obtained from closed air open water cycle (CAOW) [4]. In CAOW cycle, the moist air exiting from the dehumidifier enters the humidifier which means the mist air at the outlet of the dehumidifier and the inlet of the humidifier has the same conditions. Higher value of relative humidity means more condensation in the dehumidifier. So, the relative humidity in this cycle represents the condensation performance. Thus, GOR increases as the air relative humidity at the outlet of the dehumidifier (the inlet of the humidifier) increases . However, in open air open water cycle (OAOW), GOR increases as the inlet air relative humidity decreases as shown in Figure 2.11 [29]. The primary factor behind this increasing in the performance is that if the moist air enters the humidifier at low relative humidity (low moisture content), it will have grater potential to absorbed moisture than if it is saturated. Also, the saline water will leave the humidifier at lower temperature because of the difference between the dry and wet-bulb temperatures.

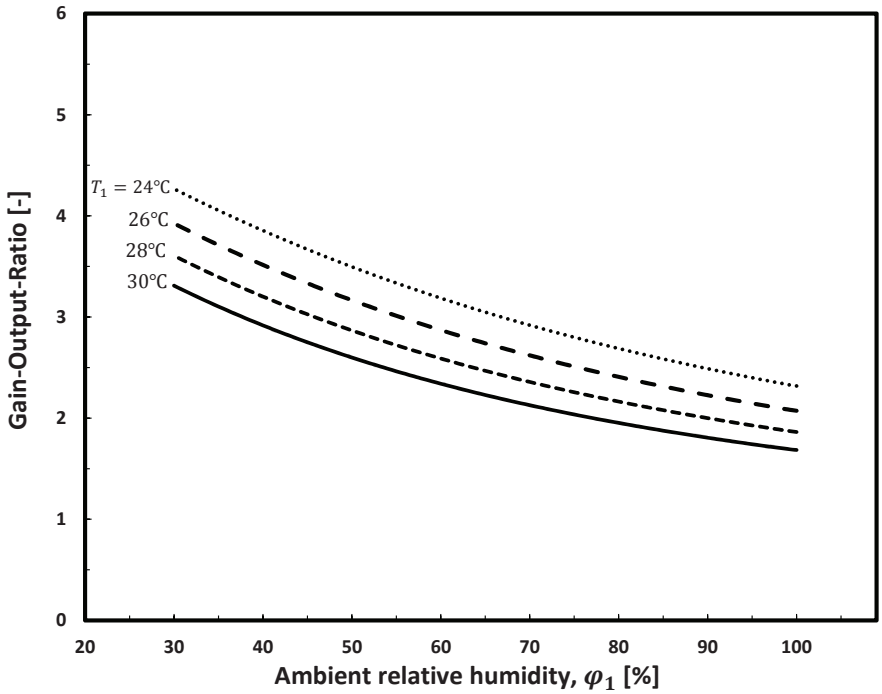

Figure. 2.10: Effect of ambient relative humidity on the performance of the system.

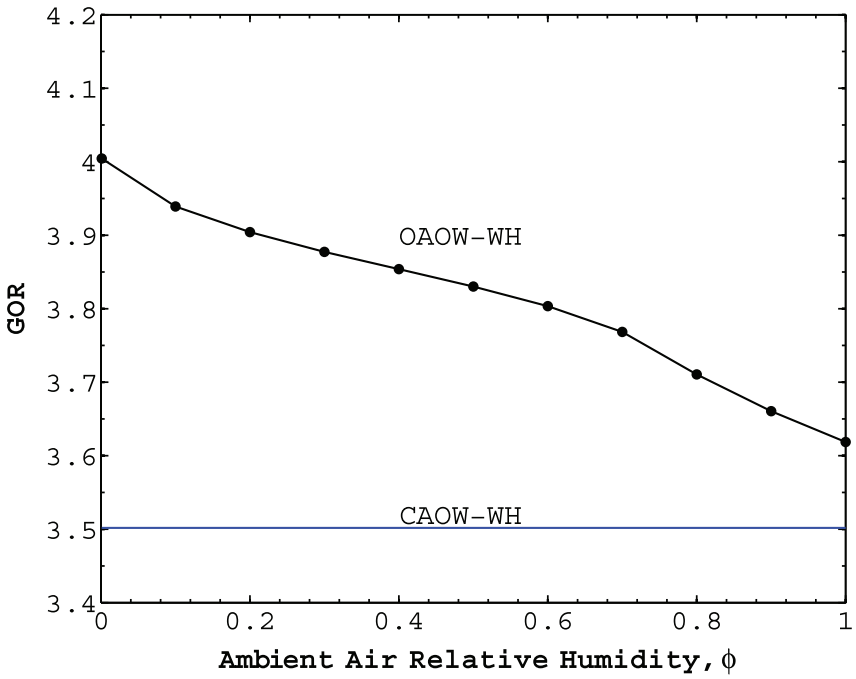

Figure. 2.11: GOR versus ambient relative humidity for OAOW-WH cycle. GOR for CAOW-WH cycle also plotted for reference [29].

2.5 Target Performance

In the previous section (Section 2.4), the performance of the cycle is evaluated under more realistic conditions which are listed in Table 2.2. In this section, the maximum performance of the system is evaluated by ignoring the irreversibly in the humidifier, dehumidifier and heat exchanger where the turbocharger is only the design constrain. So, effectiveness of 100% and pressure losses of 0.0 kPa in these components are used to evaluate the maximum performance where the rest parameters are kept as same as listed in Table 2.2. Figures 2.12-2.15 show the effect of pressure ratio; mass flow rate ratio; inlet air and water temperatures and inlet air relative humidity on the performance of the system (GOR); respectively. It is clear that the variations of the performance have similar trends as well as the results discussed in the previous section. The peak performance (GOR) under the given boundary conditions is 13.6 at pressure ratio of 1.7 and mass flow rate ratio of 8.2. The maximum performance (GOR) obtained is 27 at inlet air temperature (T_1) of 20°C and inlet water temperature of 31°C. Moreover, the performance of the system (GOR) could exceed 30, if the performance parameters and boundary conditions are optimized at the maximum performance.

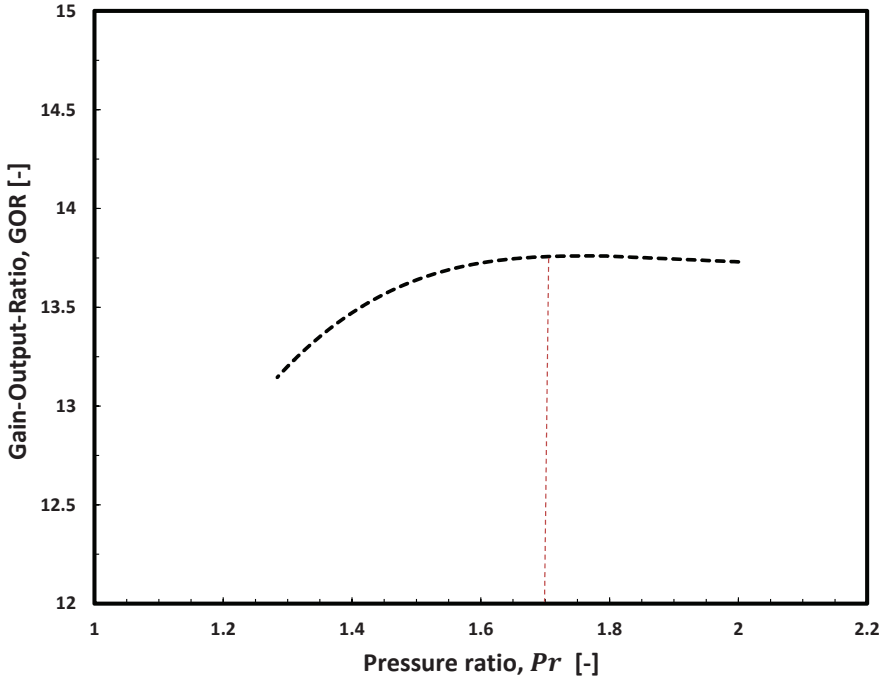

Figure. 2.12: Effect of pressure ratio on the maximum performance of TDMC-HDH system.

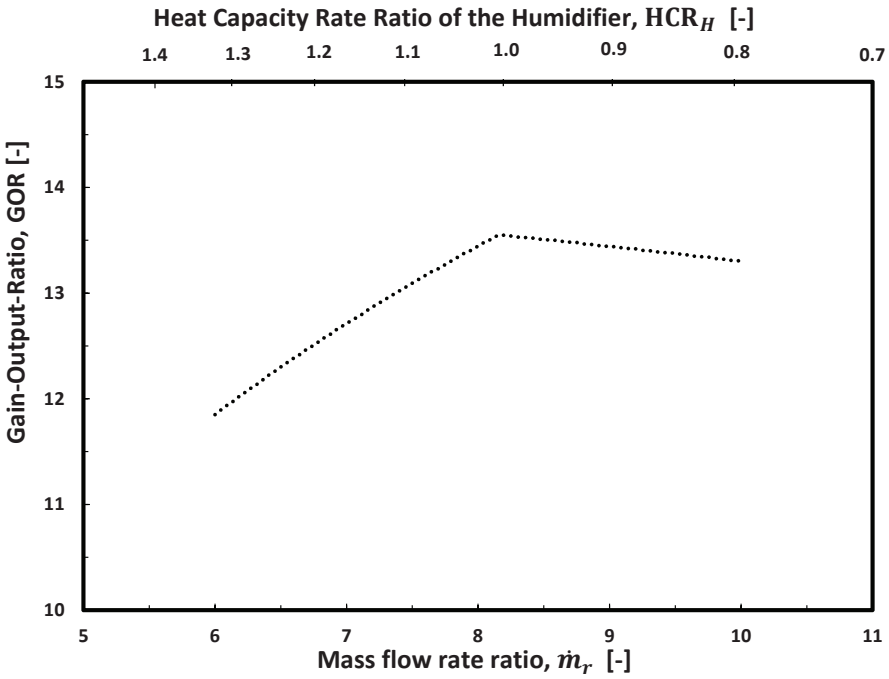

Figure. 2.13: Effect of mass flow rate ratio on the maximum performance of TDMC-HDH system.

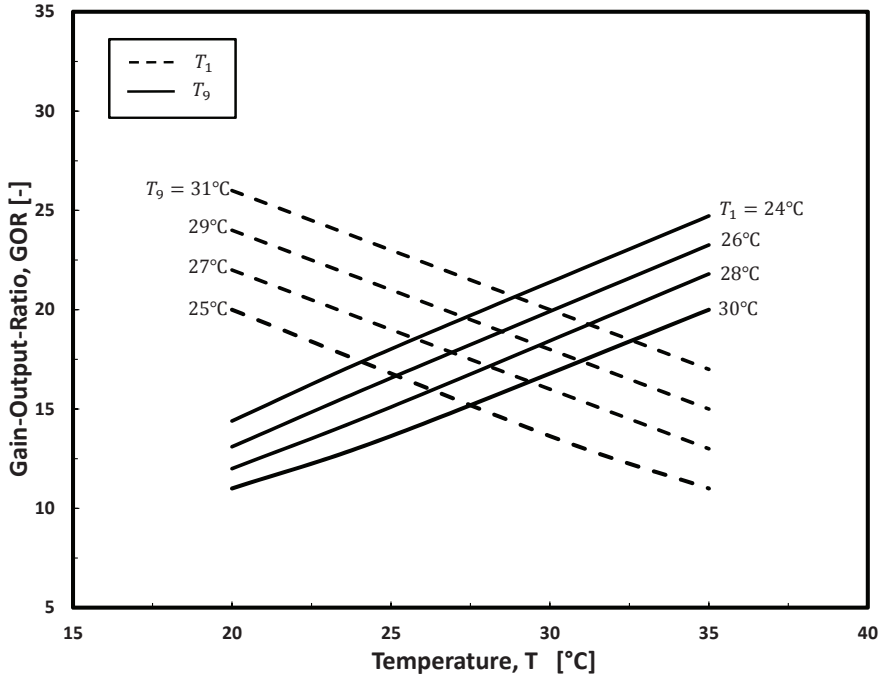

Figure. 2.14: Effect of inlet air and water temperatures on the maximum performance of TDMC-HDH system.

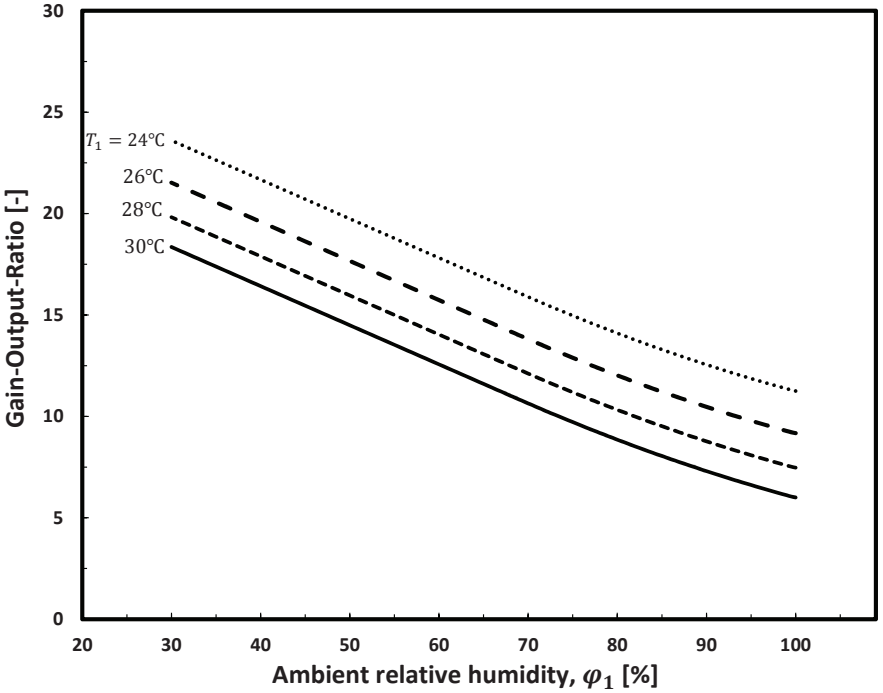

Figure. 2.15: Effect of inlet air relative humidity on the maximum performance of TDMC-HDH system.

CHAPTER 3

MULTI-STAGE BUBBLE COLUMN HUMIDIFIER

In this chapter, an experimental investigation is conducted in order to evaluate the performance of a multi-stage bubble column humidifier. The effect of different parameters on the humidifier performance and the pressure losses are studied. These parameters include air superficial velocity, mass flow rate ratio, number of stages, water gate height and sparger profile.

3.1 Terminology used

- Air superficial velocity (V_{SG}): the ratio of the volumetric flow rate of the air ($\dot{\forall}_a$) to the cross sectional area of the bubble column (A_{column}) [30, 31],

$$V_{SG} = \frac{\dot{\forall}_a}{A_{column}} \tag{3.1}$$

- Mass flow rate ratio ($\dot{m}_r$): the ratio of the mass flow rate of the water stream ($\dot{m}_w$) to the mass flow rate of the air stream ($\dot{m}_a$),

$$\dot{m}_r = \frac{\dot{m}_w}{\dot{m}_a} \tag{3.2}$$

3.2 Multi-stage bubble column humidifier design

In order to conduct the multi-stage bubble column humidifier experiment, different designs have been developed. However, among these designs, only one design was selected to conduct the experiment. This chapter will discuss the detailed description of the multi-stage bubble column humidifier design and experiment setup.

3.2.1 Frame

The column of the multi-stage humidifier is constructed out of 277mm Plexiglas pipe which is a transparent thermoplastic material with thermal conductivity of 0.19 W/m.K. Using such a material will be helpful to see what happens inside the column while the experiment is running. Also, due to its low thermal conductivity, heat losses from the system will be minimized.

3.2.2 Sparger

The sparger or perforated plate is made of a PVC sheet, 18mm thick. Three different configurations for the sparger have been tested as shown in Figure 3.1. These three spargers differ in their number of holes, pitch size and open area ratio where open area is the ratio between the total area of the holes and total sparger area. Table 3.1 shows the configuration parameters for each sparger.

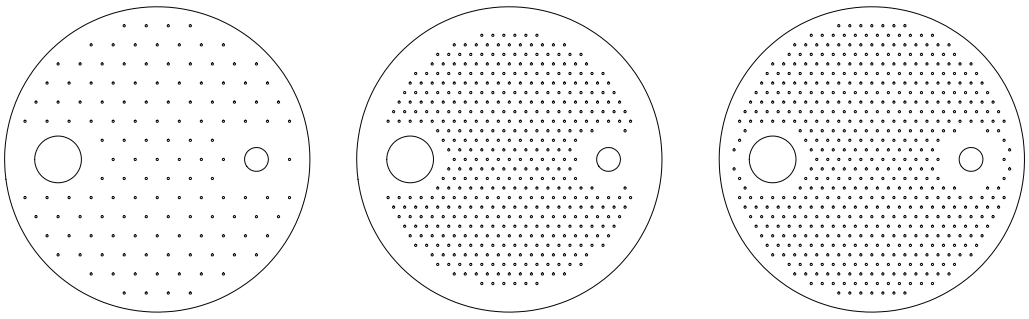

(a) (b) (c)

Figure. 3.1: Tested spargers

Table. 3.1: Spargers profile

Sparger dia-	Sparger -meter [mm]	Hole dia- -meter [mm]	Open area ratio [%]	Number of holes	Pitch size [mm]
a	277	2	0.68	130	20
b	277	2	2.22	425	10
c	277	2	2.71	520	10

Holes are designed in a way to reduce the dynamic pressure drop. Figure 3.2 illustrates that the diameter of the holes extends 5mm from the entrance till 2mm before the upper surface of the sparger. Then, the diameter of the hole narrows to 2mm till the upper surface of the sparger.

The sparger is fitted in the column by an embedded O-ring around the sparger as shown in Figure 3.3. The O-ring and groove design have been selected according to MARCO RUBBER & PLASTIC PRODUCTS, INC standards [32, 33]. There are two main advantages of using this technique. The first one is to prevent air and water leakages. By using the O-ring fitting, there will be no leakage between the stages or to the surroundings. The second advantage is to make the device installation easier and faster.[32]

The sparger includes a water gate holder which is also designed using an em-

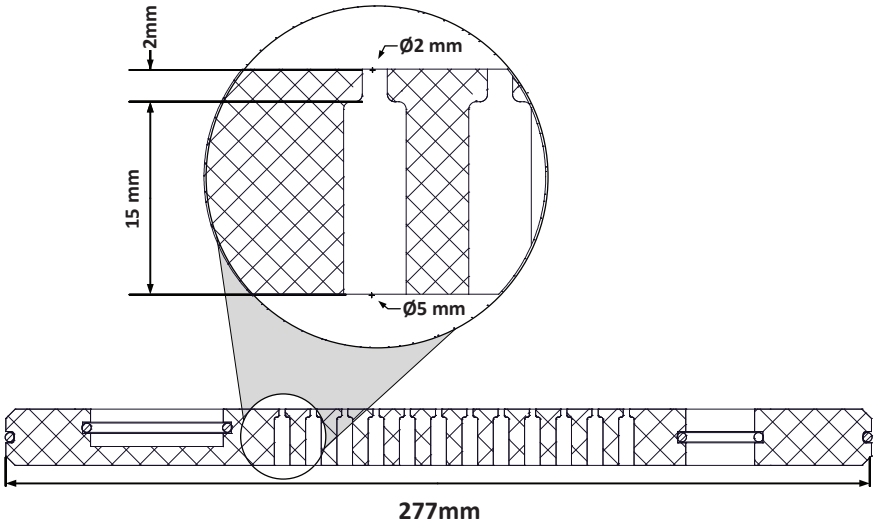

Figure. 3.2: Holes design

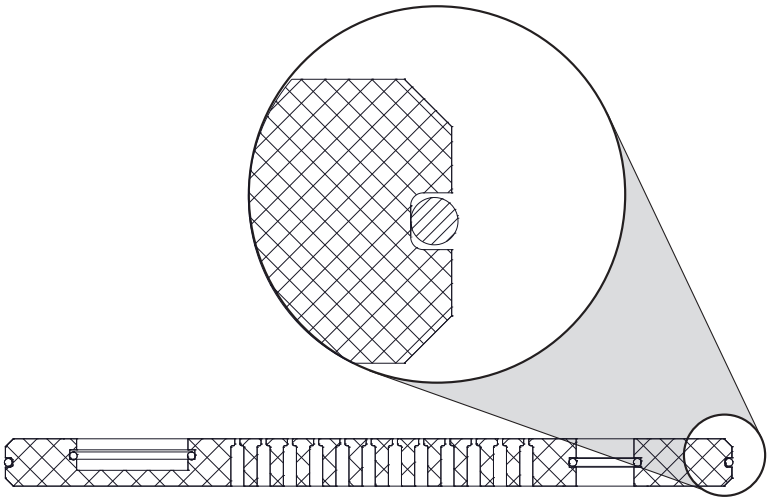

Figure. 3.3: Embedded O-ring around the sparger

bedded O-ring as shown in Figure 3.4a. The advantage of using this technique here is to control the height of the water gate easily. Also, the sparger includes a holder for the base cup of the water gate as shown in Figure 3.4b.

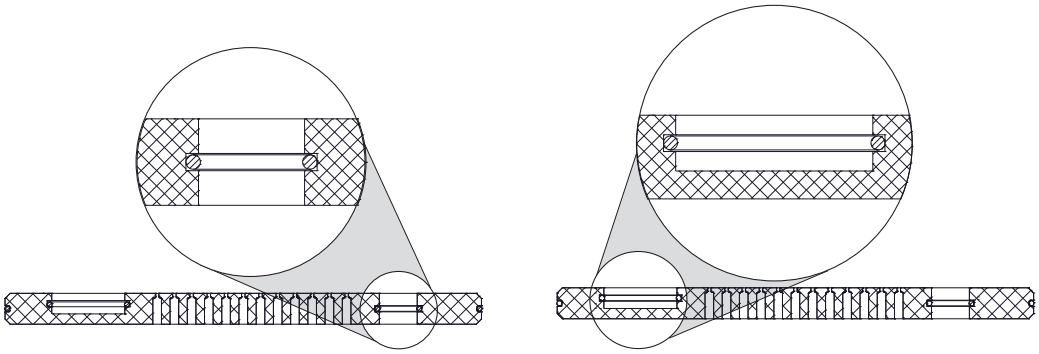

(a) Holder of water gate **(b)** Holder of water gate base

Figure. 3.4: Embedded O-ring for water gate and base cup holder

Figure 3.5 illustrates how the water gate and its base are installed in the sparger.The water gate rises above the sparger and contains a cone cup on its top tip to collect the water without bubbles. Then the water goes through this gate to the other stage. The bottom tip of the water gate is installed in the base cup to force the air stream to go to the other stage through the sparger instead of the water gate.

3.2.3 Upper and lower plates

Upper and lower plates are, as well as the sparger, made of 18mm thick CPVC. Also, they fitted in the column using an embedded O-ring. Figure 3.6a shows that the upper plate includes the air exit gate and the water entrance gate, whereas the lower plate includes the air entrance gate, water exit gate, and the base cup for the water gate of the first stage as shown in Figure 3.6b.

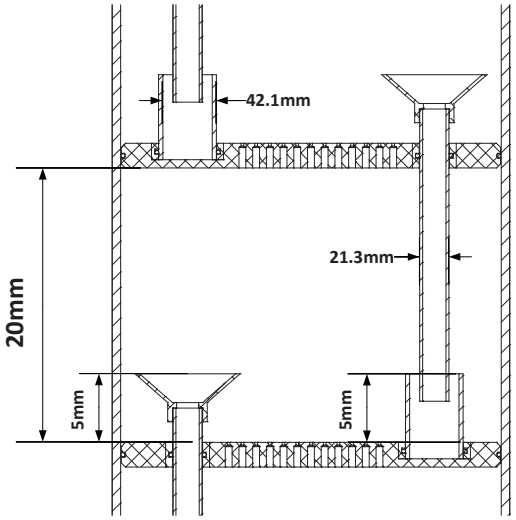

Figure. 3.5: Assembling the water gate and its base cup in the spargers

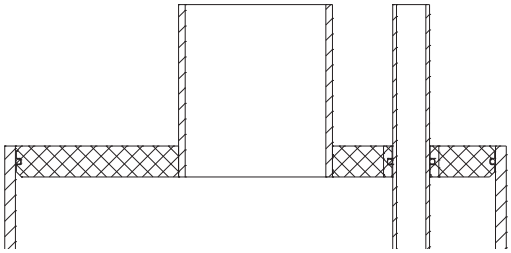

(a) Upper plate.

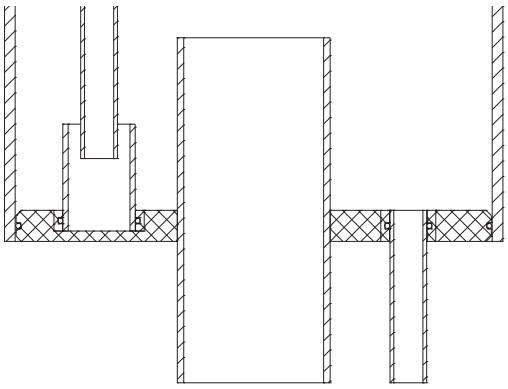

(b) Lower plate.

Figure. 3.6: Upper and lower plates design.

3.3 How it works

There are two counter-flow streams in the humidifier. One stream is the water that comes from the dehumidifier and the other stream is the moist air that comes from ambient. In the humidifier, mass and heat are transferred simultaneously from saline water to the air stream. Figure 3.7 shows how the water and air streams flow in the bubble column humidifier.

3.3.1 Water stream

The hot water stream enters the bubble column through the water entrance gate which ends in a base cap to prevent the air from entering the water entrance gate. Then, the water overflows the base cup and flows over the sparger until reaching the cone cup to be collected there. After this, it flows through the water gate to the other stage. The same thing will be repeated in the next stages until it reaches the lower plate.

3.3.2 Air stream

The air enters the bubble column humidifier at the ambient conditions. Then, the air is sparged through the sparger to form bubbles in a pool of hot water. In this direct contact process, mass and heat are transferred simultaneously from the hot water to the air bubbles. Then, the humid air moves to the next stages in the same manner until reaching the air exit gate.

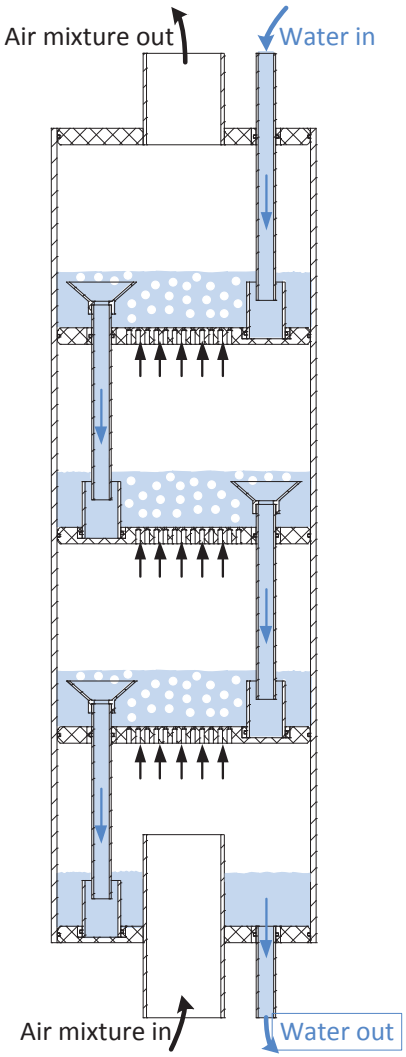

Figure. 3.7: Multi-stage bubble column humidifier

3.4 Experimental setup and procedures

3.4.1 Experimental setup

In order to study the performance of a multi-stage bubble column humidifier, a laboratory scale setup was designed and built. Figure 3.8 shows a schematic diagram of the experimental setup used in the study. The setup consists of an air blower, an instant water heater, and a multi-stage bubble column. The air is delivered to the bubble column humidifier (17) by an 800 W air blower (1) with a maximum volumetric flow rate of 4.5 m^3/min. Then, the air is humidified and heated up in the bubble column humidifier by direct contact with the water stream, then leaves from the outlet gate. The water is supplied from a tap through 1/2″ CPVC pipe. Then, the water is heated up using an instant water heater (15) with maximum power of 7.5 kW. The water heater is supported by a proportional-integral-derivative controller (PID controller) in order to provide a constant temperature for the water stream. The hot water enters the bubble column humidifier through the upper plate and leaves through the lower plate.

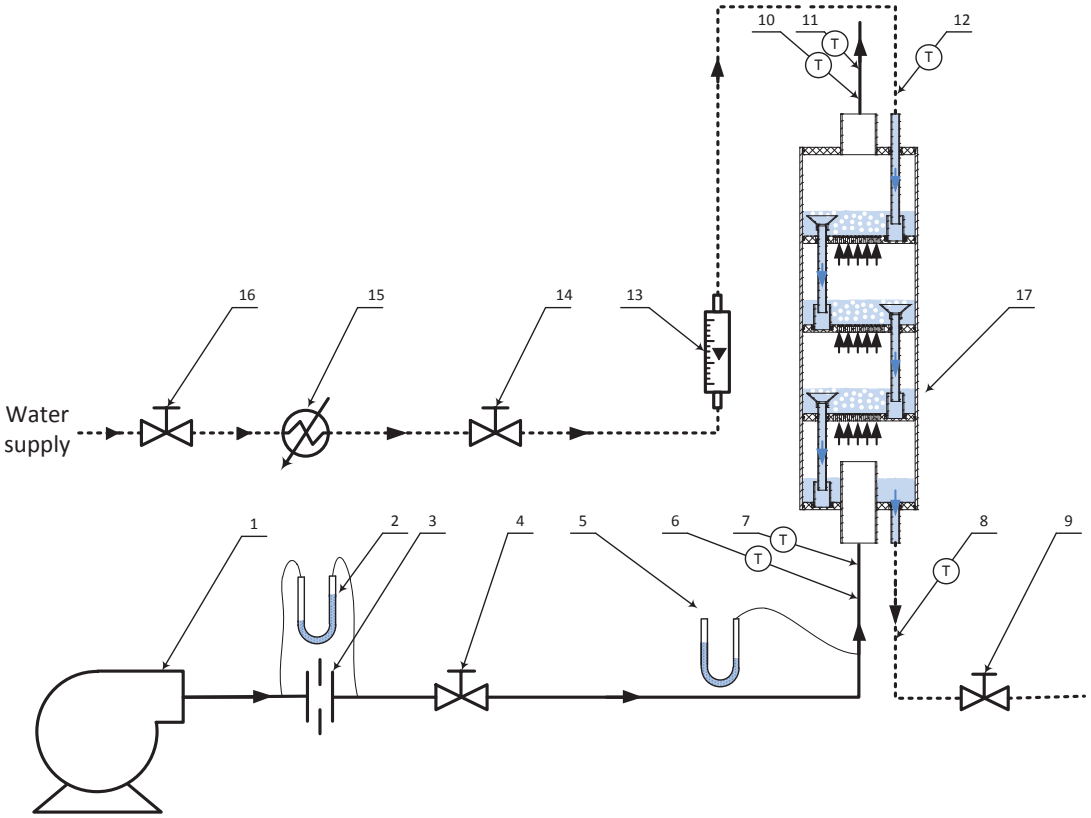

Figure. 3.8: Schematic diagram of experimental setup: **(1)** Air blower, **(2, 5)** Manometer, **(3)** Orifice meter, **(4, 9, 14, 16)** Valve, **(6, 7, 8, 10, 11, 12)** Thermocouple, **(13)** Rotameter, **(15)** Water heater, **(17)** Bubble column humidifier.

3.4.2 Procedures

1. The experiment starts by blowing the air into the bubble column humidifier using the blower because if the water flows first, it will go through the sparger holes.

2. The volumetric flow rate of the air stream is adjusted to the desired volumetric flow rate using the orifice meter (3) and throttle valve (4). In Appendix A, the orifice meter design is described in detail.

3. After blowing the air stream, the water supply valve (16) is opened. Throttle valve (14) is used to control the volumetric flow rate of water which is measured using a rotameter (13).

4. The water heater (15) is turned on and set to the desired temperature.

5. The system is observed until it reaches steady state conditions. It usually takes from 15 min to 20 min to reach steady state conditions.

6. While the experiment is running, the valves, rotameter, and orifice meter are continuously monitored and readjusted to the desired flow rate.

7. At steady state conditions, the values of water temperatures at the inlet and outlet of the water stream and air dry-bulb/wet-bulb temperatures at the inlet and outlet of the air stream are recorded using thermocouples (12, 8, 6, 7, 10 and 11) respectively. The value of pressure drop in the bubble column humidifier is recorded using a manometer (5).

3.4.3 Measurement devices

The thermocouples used in the experiment are of K-type. The thermocouples are connected to a data logger with accuracy of ± 0.5°C. The rotameter used for water volumetric flow rate measurement has a range of $1 - 7$ LPM ($16.7 - 116.7$ cm^3/s) with accuracy of ± 0.25 LPM (4.17 cm^3/s). The pressure difference across the orifice meter and the pressure drop in the bubble column humidifier are measured using water manometers with accuracy of ± 1 mm.

The approach described by Coleman and Steele [34] was performed, in order to estimate the uncertainty in the presented results, as described in Appendix C.

The uncertainty in the measurements is defined as the root sum square of the bias error of the instrumentation and the precession error observed. Accordingly, the resulting uncertainties are ±0.67 cm/s, ±0.283 kg/s, ±0.83%, ±0.85% and ±2.52% in the calculated air superficial velocity, mass flow rate ratio, inlet air relative humidity, outlet air relative humidity and humidifier effectiveness.

3.5 Results and discussion

3.5.1 Sparger profile selection

Three different spargers were used in this experiment. The design of these three spargers is discussed in Section 3.2.2. Sparger (c) does not work efficiently since there is a water leakage through the boundary openings. This could be attributed to the shear stress near the wall of the column which results in a low air velocity at that region. So, sparger (c) is not considered in this investigations.

Figure 3.9 shows the effect of the sparger profile on the humidifier effectiveness at different mass flow rate ratios. It is clear that the humidifier effectiveness is slightly affected by the sparger profile where the effectiveness for sparger (a) is only 2.5% higher than sparger (b). However, as shown in Figure 3.10, the pressure losses in sparger (a) is much higher (more than 400%) than sparger (b) because the number of holes is fewer which means higher air jet velocity through the holes and higher dynamic pressure losses. For this reason, sparger (b) was selected for further investigations.

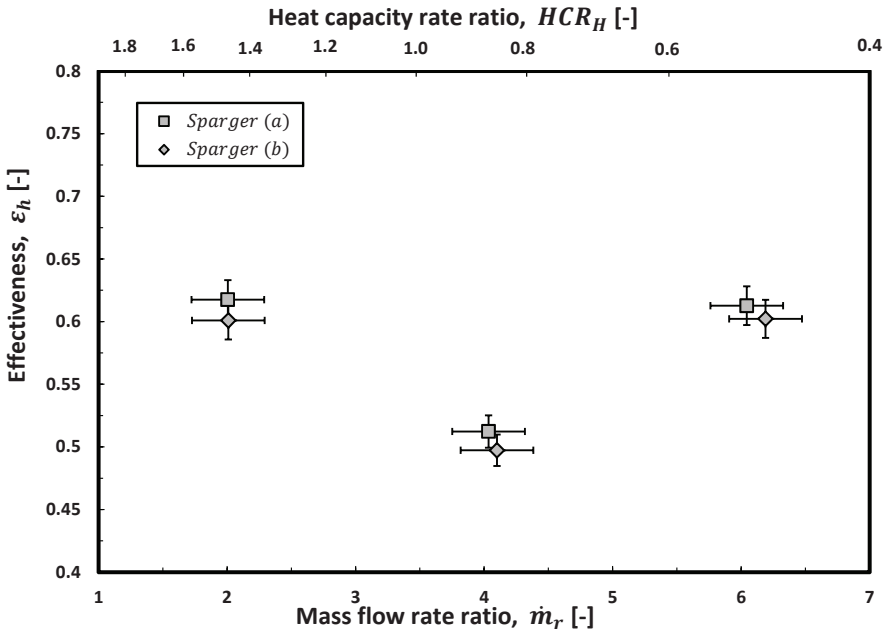

Figure. 3.9: Effect of sparger profile on the humidifier effectiveness. Boundary conditions: $T_{a,i}$ = 34.2°C; $\phi_{a,i}$ = 55%; $T_{w,i}$ = 63.1°C; P = 101.3kPa; h = 5cm; V_{SG} = 25cm/s; single-stage.

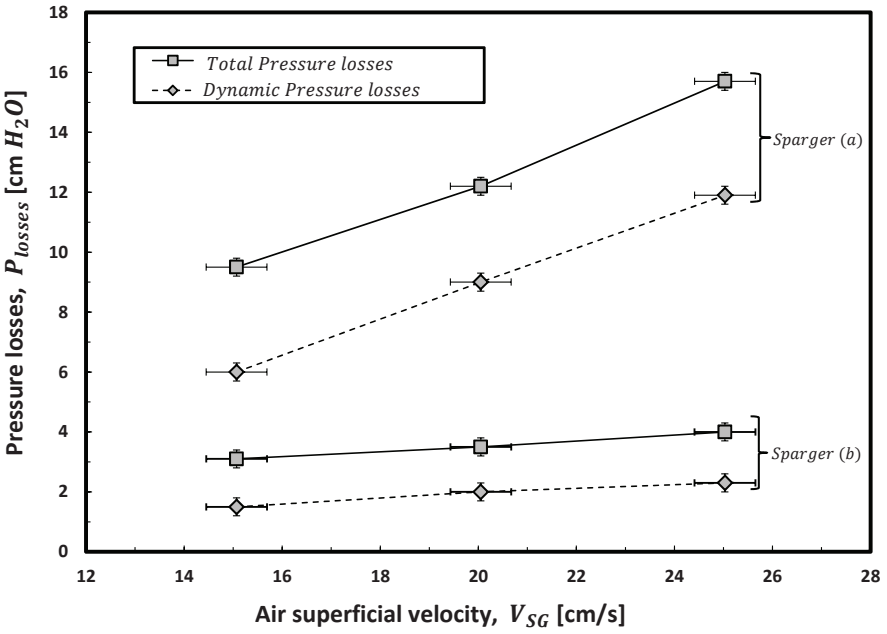

Figure. 3.10: Effect of sparger profile and air superficial velocity on the pressure drop. Boundary conditions: $T_{a,i}$ = 34.2 °C; P = 101.3 kPa; h = 5 cm; $\dot{m}_r$ = 2; single-stage.

3.5.2 Effect of the mass flow rate ratio on the humidifier performance

Figure 3.9 illustrates the effect of the mass flow rate ratio on the humidifier performance. It is clear that the effectiveness is minimum at $\dot{m}_r = 4$ where heat capacity rate ratio (HCR_H) is close to unity (thermal balanced condition). The reason for getting this low value of effectiveness at balanced condition could be explained by recalling the definition of HCR_H (Eq. 2.6). If HCR_H is greater than or less than unity, one of the streams (air or water) in the humidifier will have a greater heat capacity rate than the other stream as shown in Figure 3.11a and Figure 3.11b. Thus, the potential of heat and mass transfer is greatly increased, which results in a higher effectiveness. On the other hand, the potential of heat and mass transfer is minimum as HCR_H approaches unity since the two streams have the same heat capacity rate as illustrated in Figure 3.11c. So, for fixed size of heat and mass exchange devices, the minimum effectiveness is obtained at HCR= 1.

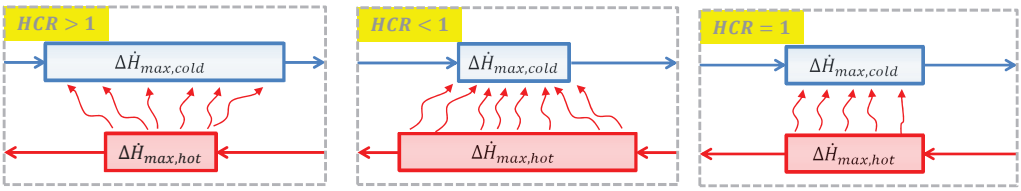

(a) HCR> 1 **(b)** HCR< 1 **(c)** HCR= 1

Figure. 3.11: Heat and mass transfer for different heat capacity rate ratios.

3.5.3 The importance of the insulation

For a humidifier heat losses to the surrounding reduces the potential of heat transfer between the water and air. This reduces the effectiveness of the system. So, insulating the humidifier is necessary to avoid performance degradation due to heat losses to the surrounding.

In this part, heat losses effect on the humidifier's effectiveness is analysed and evaluated experimentally by applying the energy balance on the humidifier as follow:

$$\underbrace{\dot{m}_{da}(h_{a,i} - h_{a,o})}_{\Delta\dot{H}_a} - \underbrace{(\dot{m}_{w,o}h_{w,o} - \dot{m}_{w,i}h_{w,i})}_{\Delta\dot{H}_w} = \dot{Q}_{loss} \tag{3.3}$$

where $\Delta\dot{H}_a$ represents the difference in the total enthalpy rate for the humid air stream and $\Delta\dot{H}_w$ represents the difference in the total enthalpy rate for the water stream.

Expanded polyethylene with thermal conductivity of 0.034 W/m.K is used as an insulator. Figure 3.12 illustrates the influence of insulating the humidifier on the non-dimensional heat losses (ratio of rate of heat lost through humidifier's wall to rate of heat transferred between the two streams). It is clear that the insulation reduces the heat loss by 50%. So, for all experiments, the humidifier is operated with insulation.

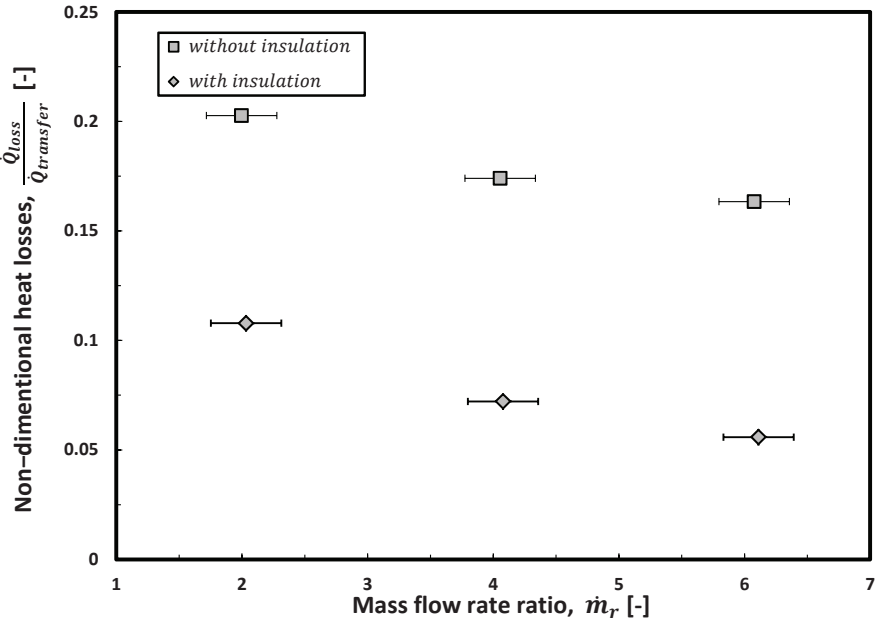

Figure. 3.12: Heat losses with and without insulation. Boundary conditions: $T_{a,i} = 34.2$ °C; $\phi_{a,i} = 55\%$; $T_{w,i} = 63.1$ °C; $P = 101.3$ kPa; $h = 5$ cm; $V_{SG} = 25$ cm/s; single-stage.

3.5.4 Foam formation

Under certain conditions, foam is formed in the bubble column where the air bubbles are dispersed throughout the water. There are two main factors causing the foam formation. These factors are the air superficial velocity and the water gate height. At different water gate height (1-5cm) and high superficial velocity (greater than 20cm/s for this setup), the velocity at the nozzle is high enough to form many dispersed bubbles which form foam in the bubble column as shown in Figure 3.13. However, at water gate height of 5cm and low air superficial velocity, there is no foam formation because the water accumulates over the sparger before foam starts forming as shown in Figure 3.14. Nevertheless, if the water gate height is reduced to less than 2.6cm, the foam will be formed at superficial velocity of 15cm/s.

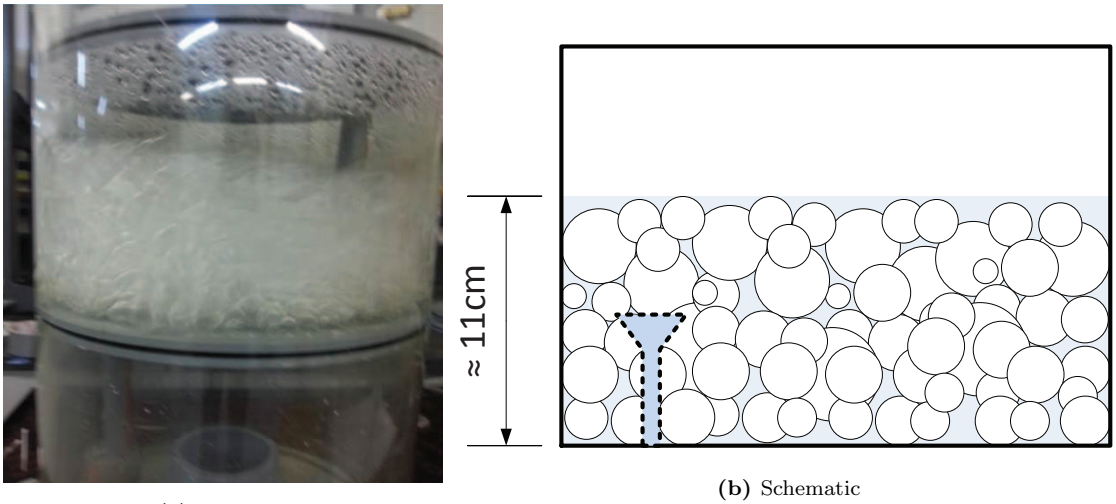

(a) Snapshot **(b)** Schematic

Figure. 3.13: Foam formation at $V_{SG} = 25$cm/s and $h = 5$cm.

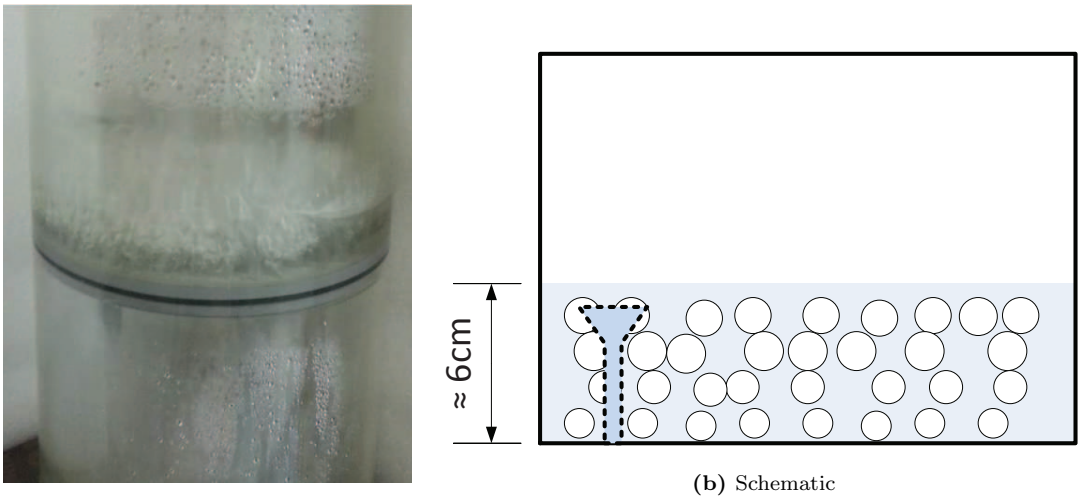

(a) Snapshot **(b)** Schematic

Figure. 3.14: Normal bubble flow at $V_{SG} = 15$cm/s and $h = 5$cm.

3.5.5 Effect of air superficial velocity and water gate height

Figure 3.15 shows the effect of the water gate height at different mass ratios on the humidifier's effectiveness. If the bubble column humidifier is operated at relatively high air superficial velocity, the humidifier is slightly affected by the height of the

water gate as shown in Figure 3.15a and Figure 3.15b. At these two superficial velocities, foam is formed in the bubble column which increases the water height and the gas holdup [35]. Therefor, with higher water (in foam formation), the time and surface of contact are increased enhancing heat and mass transfer. However, at low air superficial velocity, there is a drop in the effectiveness at 5cm of height as shown in Figure 3.15c since in this case there is no foam formation. Further discution on foam formation is presented in Section 3.5.4

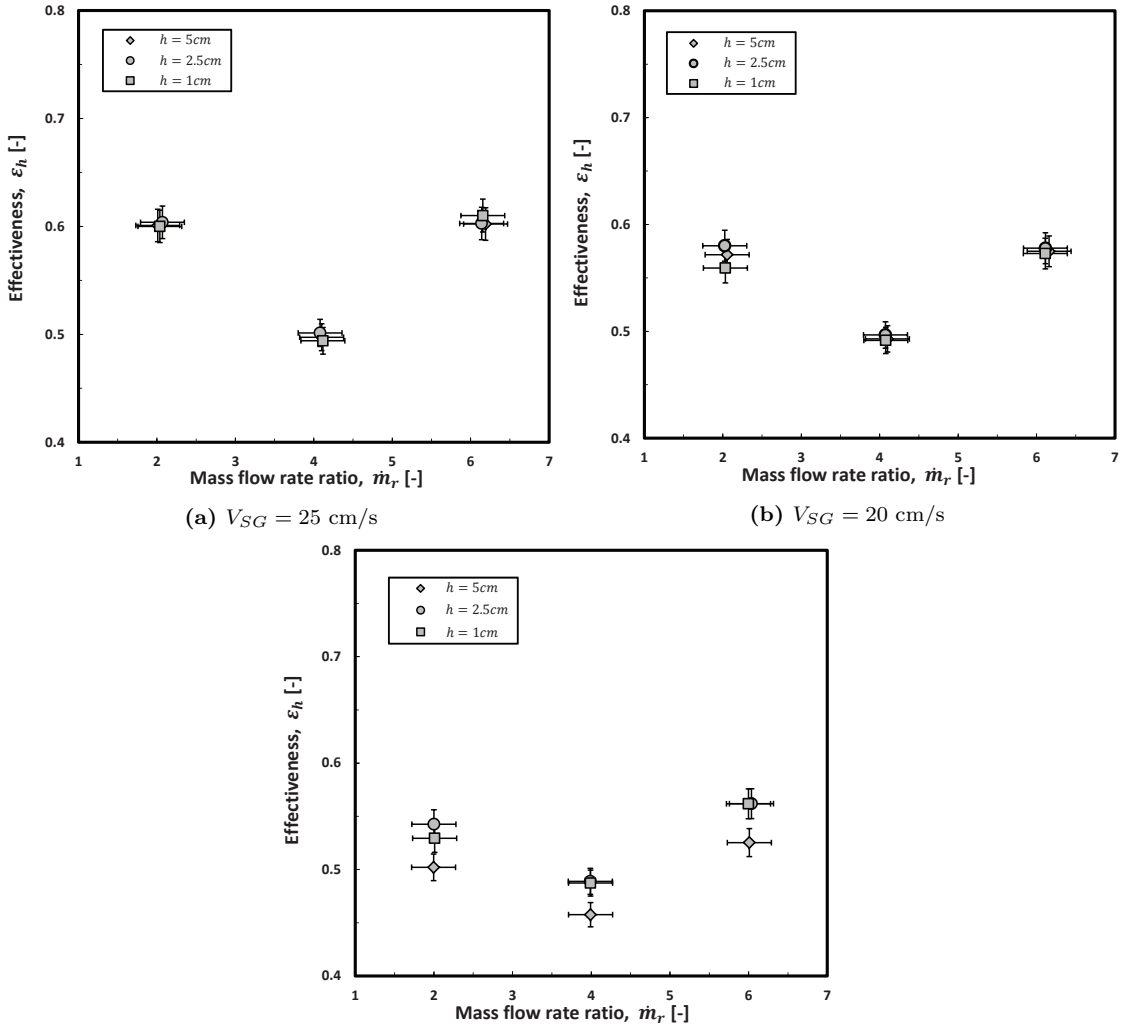

(a) $V_{SG} = 25$ cm/s

(b) $V_{SG} = 20$ cm/s

(c) $V_{SG} = 15$ cm/s

Figure. 3.15: Effect of water gate height on the humidifier effectiveness. Boundary conditions: $T_{a,i} = 34.2$ °C; $\phi_{a,i} = 55\%$; $T_{w,i} = 63.1$ °C; $P = 101.3$ kPa; single-stage.

3.5.6 Effect of the number of stages on the humidifier's effectiveness

Up to this point, investigations are carried out on a single-stage bubble column humidifier. It was clear that its performance is not promising for HDH applications, being 63% at most. Although, the two streams flow counter-currently, the exiting water and air temperatures are almost the same as illustrated in Figure 3.16a because they mix homogeneously in the bubble column. So, implementing a multi-stage bubble column humidifier would resolve this issue. In the multi-satge bubble column humidifier, the temperature paths of air and water are segmented to enhance the air temperature to reach higher temperature as shown in Figure 3.16b. Also, the temperature difference is reduced at each stage which reduce the irreversibility in the system.

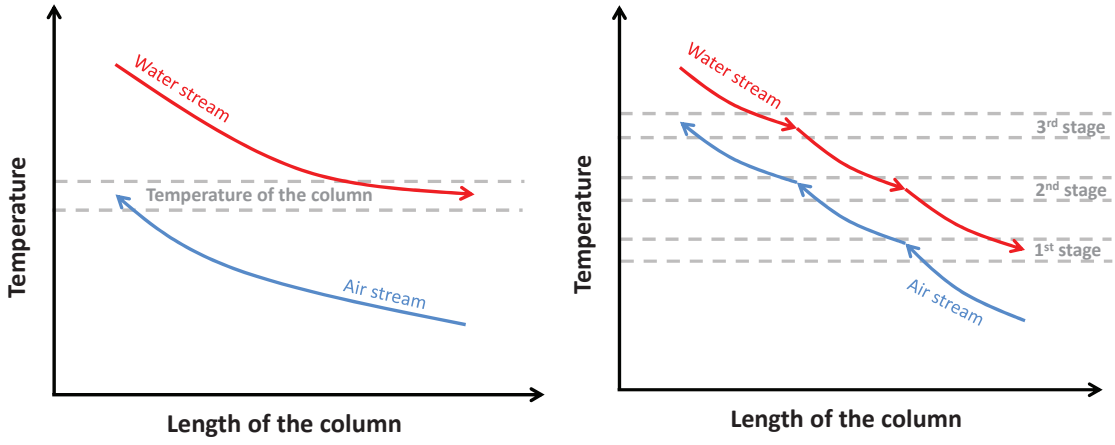

(a) Single stage **(b)** Multi-stage

Figure. 3.16: Temperature path along the humidifier column.

Experimental result (Figure 3.17) shows the effect of the number of stages on the humidifier's effectiveness. As we increase the number of stages, the effec-

tiveness increases. The improvement in the effectiveness is more than 30% for a two-stage and more than 45% for a three-stage humidifier. So, the number of stages has a significant effect on the effectiveness of the humidifier. However, we can't go to infinite number of stages since the pressure losses is also proportional to the number of stages (see Section 3.5.7), which increases the irreversibility of the system.

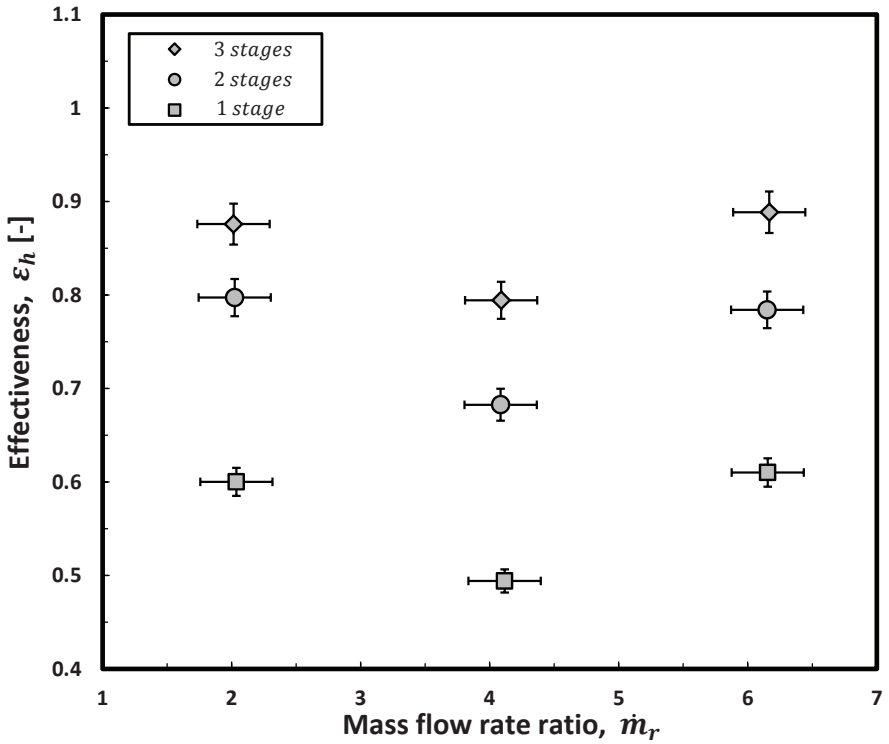

Figure. 3.17: Effect of the number of stages on the humidifier effectiveness. Boundary conditions: $T_{a,i}$ = 34.1 °C; $\phi_{a,i}$ = 55%; $T_{w,i}$ = 63.1 °C; P = 101.3 kPa; h = 1 cm; V_{SG} = 25 cm/s.

3.5.7 Pressure losses

Pressure losses has a significant effect on the performance of the TDMC-HDH cycle as presented in Section 2.4.1. In this section, the pressure losses in the multi-stage bubble column humidifier is studied experimentally.

Figure 3.18 shows the effect of the number of stages on the pressure drop. It is clear that the pressure drop increases linearly as the number of stages is increased. Each stage has almost the same pressure losses for the same operating conditions. The total pressure losses of the humidifier is the sum of pressure losses for all stages. The dashed line in the figure is the dynamic pressure drop which represents the major contribution of the total pressure losses. Also, it is observed that the pressure losses increases as the air superficial velocity is increased.

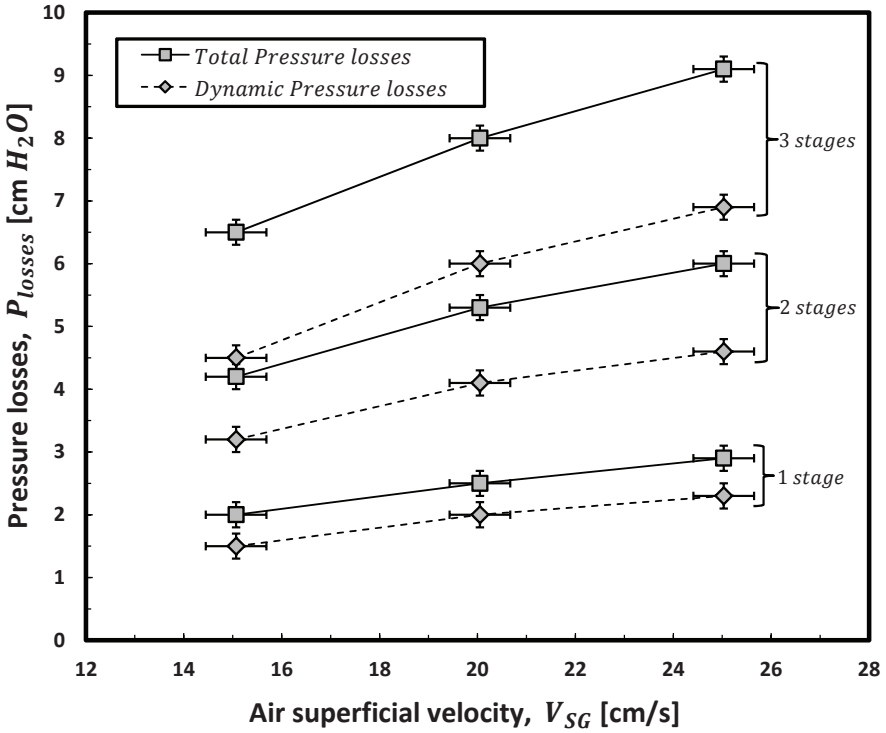

Figure. 3.18: The pressure drop in multi-stage bubble column humidifier. Boundary conditions: $T_{a,i} = 34.2$ °C; $P = 101.3$ kPa; $h = 1$ cm; $\dot{m}_r = 2$.

The air flow trough the sparger experiences sudden contraction and expansion losses as shown in Figure 3.19. These sudden contraction and expansion have fundamental losses coefficient of 0.5 and 1.0, respectively as shown in Table 3.2.

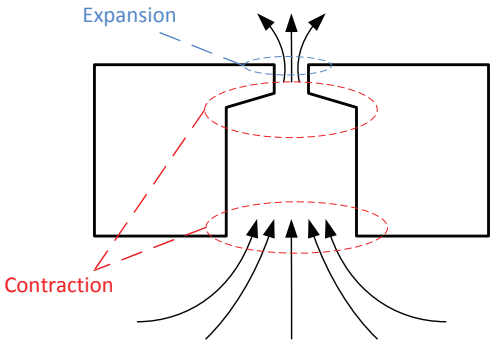

Figure. 3.19: Schematic of the nozzle.

Table. 3.2: Loss coeffecient for various transitions [36].

Description	Sketch	Additional Data		*K*
Contraction	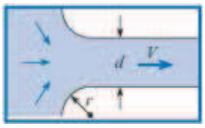	r/d		
		0.0		0.50
		0.1		0.12
		>0.2		0.03
Expansion	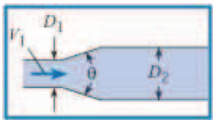	D_1/D_2	θ = 20°	θ = 180°
		0.00		1.00
		0.20	0.30	0.87
		0.40	0.25	0.70
		0.60	0.15	0.41
		0.80	0.10	0.15

Figure 3.20 shows the total pressure losses coefficient compared to the fundamental losses coefficients through the jet of the sparger at different Reynolds numbers. The total pressure losses coefficient is evluated by:

$$K = \frac{\Delta P}{\frac{1}{2}\rho V_j^2} \tag{3.4}$$

It is clear that the total pressure losses coefficient decreases linearly as Reynolds number decreases because the flow is laminar. The figure shows that there is still room for improvement since the the total pressure losses coefficient is

more than twice the fundamental losses coefficient. The difference between them could be attributed to the friction and circulation through the jet. So, the total pressure drop in the humidifier could be reduced by having a well designed perforated plate.

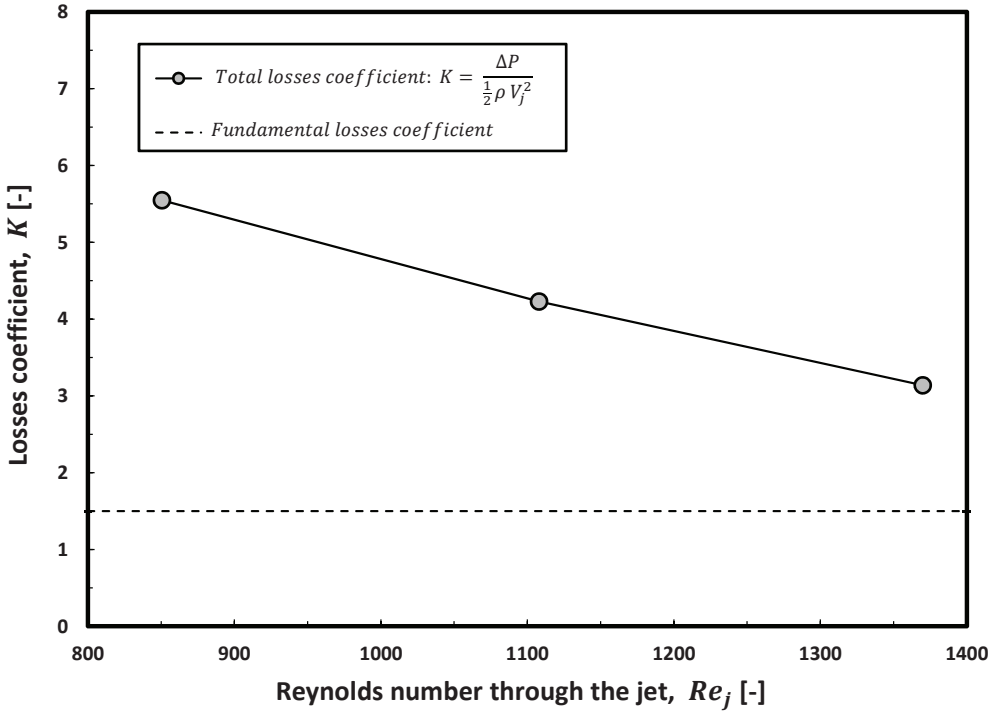

Figure. 3.20: Losses coefficient through the jet at different Re_j for single stage.

3.5.8 Relative humidity of the outlet air

Figure 3.21 presents the effect of the number of stages on the relative humidity of the outlet air. For the single-stage bubble column humidifier, the relative humidity exceeds 94%, whereas it is almost 100% for the two- and three-stage bubble column humidifier. So, the bubble column could be considered as an effective device for humidifying air. Errors for the relative humidity is less than 1% as given in Appendix C.

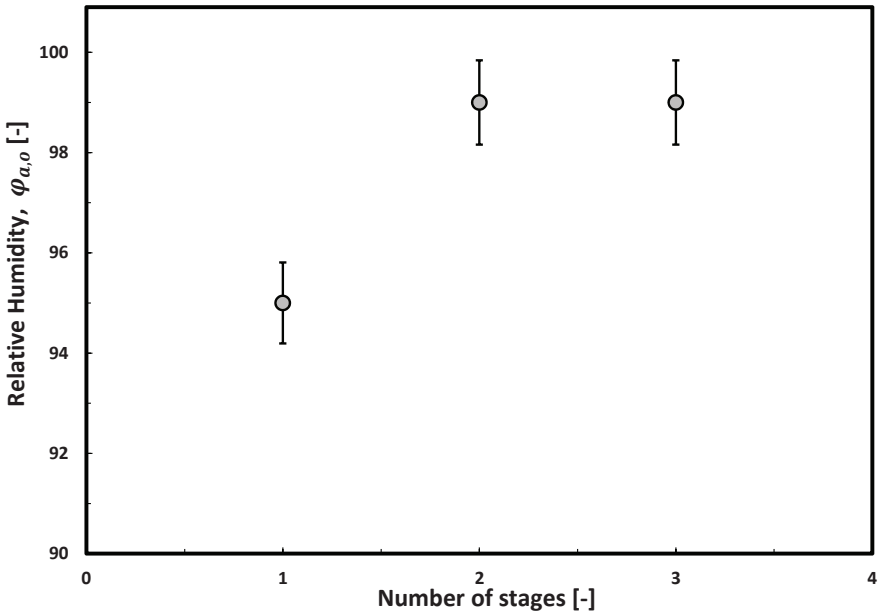

Figure. 3.21: Number of stages versus relative humidity of the outlet air. Boundary conditions: $T_{a,i} = 34.2$ °C; $\phi_{a,i} = 55\%$; $T_{w,i} = 63.1$ °C; $P = 101.3$ kPa; $h = 1 - 5$ cm; $V_{SG} = 15 - 25$ cm/s; $\dot{m}_r = 2 - 6$.

3.5.9 Comparison with packed bed humidifier

Figure 3.22 shows a comparison in effectiveness between the multi-stage bubble column humidifier and a multi-packing packed bed column carried out by Narayan et al. [37]. The comparison is conducted under similar conditions. The volume of each packing block in the packed bed humidifier is 0.07m^3, whereas the volume of each stage in the multi-stage bubble column humidifier is 0.012m^3. However, the multi-stage bubble column humidifier shows high performance compared with the packed bed humidifier. Even the three-stage bubble column humidifier has higher effectiveness than the five-packing-block packed bed humidifier, that is 0.036m^3 bubble column humidifier compared to 0.35m^3 packed bed humidifier. The current work shows an effectiveness of 85% compared to 76% by the five-packing-block packed bed humidifier.

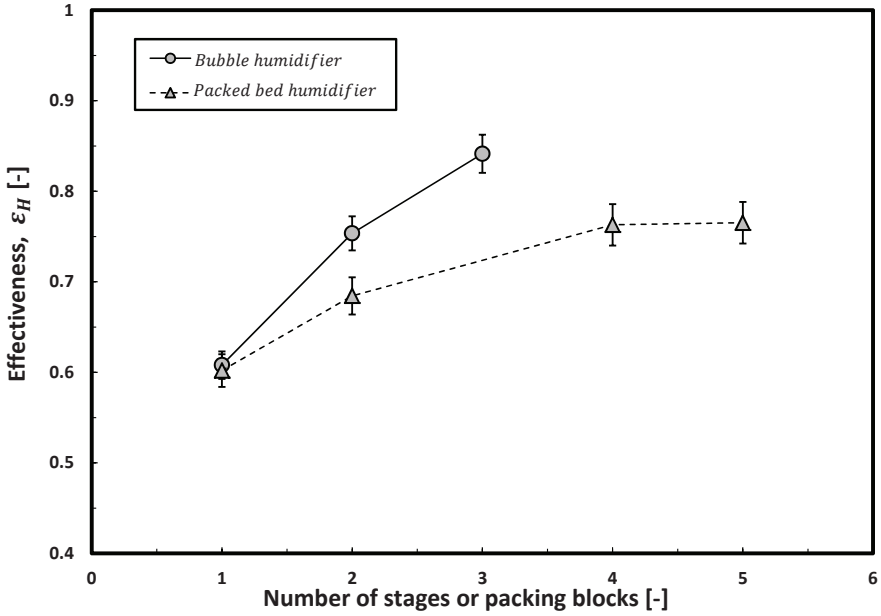

Figure. 3.22: The comparison between bubble column humidifier used in the current work and packed bed humidifier used by Narayan et al. [37]. Boundary conditions: $T_{a,i} = 33$ °C; $\phi_{a,i} = 40\%$; $T_{w,i} = 60$ °C; $P = 101.3$ kPa; $\dot{m}_r = 2.8$.

3.6 Incorporating the multi-stage bubble column humidifier in the TDMC-HDH cycle

In this section, the TDMC-HDH cycle is re-evaluated using the results obtained from the multi-stage bubble column humidifier investigation. For consistency, the baseline values mentioned before in Table 2.2 are used, except for the humidifier, the same boundary conditions of the experiment are used. So, the values used are listed in Table 3.3.

Table. 3.3: The values used to re-evaluate the TDMC-HDH cycle

Parameter	Definition	Value	Unit
T_1	temperature of air entering the system	34.2	°C
T_{10}	temperature of water entering the humidifier	63.1	°C
ϕ_1	relative humidity of air entering the system	55	%
P_H	humidifier pressure	101.3	kPa
$\dot{m}_{da}$	mass flow rate of dry air	0.1	kg/s
Pr	compressor pressure ratio	1.5	-
ε_D	dehumidifier effectiveness	90	%
ε_{HX}	heat exchanger effectiveness	85	%
η_c	compressor efficiency	78*	%
η_t	turbine efficiency	85	%
ΔP_H	pressure drop across the humidifier	0.91	kPa
ΔP_D	pressure drop across the dehumidifier	0.5	kPa
ΔP_{HX}	pressure drop across the heat exchanger	0.5	kPa

* Performance map of turbocharger used is illustrated in Appendix B.

In Table 3.4, the pressure losses and humidifier effectiveness are listed at different mass flow rate ratios. These data are obtained from the three-stage bubble column humidifier at $T_{a,i} = T_1 = 34.2$ °C; $\phi_{a,i} = \phi_1 = 55\%$; $T_{w,i} = T_{10} = 63.1$ °C; $P = 101.3$ kPa; $h = 1$ cm and $V_{SG} = 25$ cm/s.

Table. 3.4: Experimental data

	Mass flow rate ratio, $\dot{m}_r$ [−]	Pressure losses,P_{losses} [kPa]	Effectiveness, ε_H [%]
Single-stage	2	0.29	60.0
	4	0.29	49.4
	6	0.29	61.0
Two-stage	2	0.60	79.7
	4	0.60	68.3
	6	0.60	78.4
Three-stage	2	0.91	87.6
	4	0.91	80.0
	6	0.91	88.9

Figure 3.23 shows the GOR of TDMC-HDH cycle using the effectiveness of the developed multi-stage bubble column humidifier. Although the minimum effectiveness is at $\dot{m}_r = 4$ which corresponds to $\text{HCR}_H \approx 1$, the maximum GOR is obtained at this point. This can be explained by recalling the effect of the heat capacity ratio of the humidifier (HCR_H) on the GOR of the system where the irreversibility of the system is minimized at $\text{HCR}_H = 1$, further discussion is presented in Section 2.4. So, it is very important to enhance the humidifier's effectiveness at the optimum mass ratio (where $\text{HCR}_H = 1$).

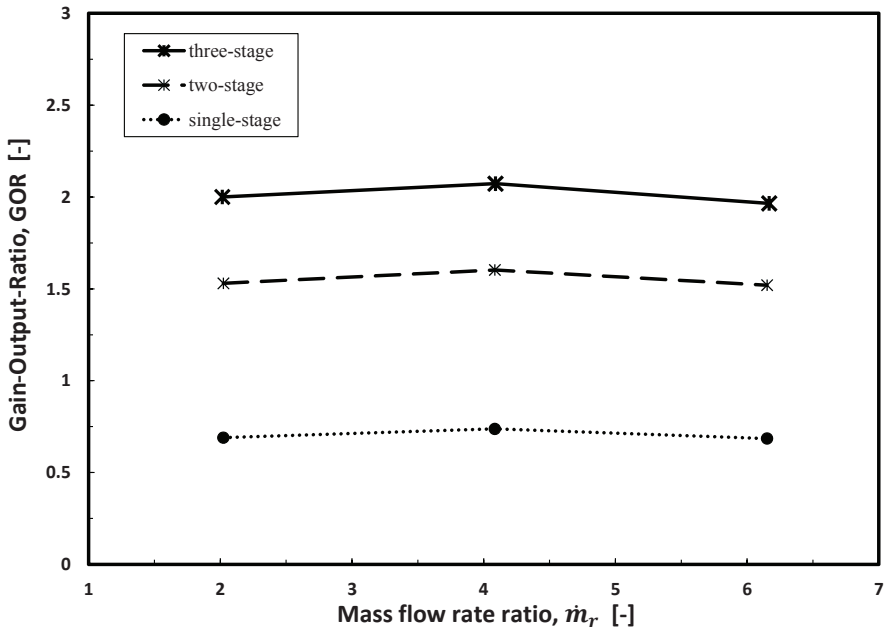

Figure. 3.23: GOR of TDMC-HDH cycle using the developed multi-stage bubble column humidifier.

CHAPTER 4

CONCLUSION AND FUTURE SCOPE

4.1 Conclusion

1. A novel desalination system has been described. It is an improvement of a varied pressure HDH system.

2. Effect of various parameters on the overall performance of the system (GOR) have been presented and discussed. These parameters include: compressor pressure ratio; pressure losses in the system's components; humidifier, dehumidifier and heat exchanger effectivenesses; compressor and turbine efficiencies; and ambient conditions.

3. Under optimized conditions, the performance of the reversible TDMC-HDH system (GOR) could exceed 30.

4. From the analysis, it is essential to have a very effective humidifier, dehumidifier and heat exchanger to obtain a reasonable GOR.

5. An experimental investigation on a novel design of the multi-stage bubble column humidifier is presented in this work. The effect of the sparger profile, heat insulation, water gate height, air superficial velocity, and mass flow rate ratio on the humidifier's effectiveness, pressure losses, and relative humidity were studied in this experiment. The conclusion of this study can be summarized in the following points:

   (a) The design of the sparger profile is a very critical issue. There is a minimum nozzle velocity ($V_{nozzle,min}$) where two undesirable cases might occur:

   - If $V_{nozzle} >> V_{nozzle,min} \Rightarrow$ High pressure losses
   - If $V_{nozzle} << V_{nozzle,min} \Rightarrow$ Water leaks through the nozzles

   There are several parameters affecting $V_{nozzle,min}$. These parameters include air superficial velocity, water gate height, and sparger design (# of holes, diameter of nozzles and area ratio). In this experiment, $V_{nozzle,min} \approx 7$ m/s.

   (b) The foam formation phenomena enhances the effectiveness. Since this phenomena is existed at high air superficial velocity and low water gate height, operating the humidifier under these two conditions is preferable.

(c) The improvement in the effectiveness is more than 30% for the two-stage and more than 45% for the three-stage humidifier. Maximum effectiveness obtained is 88.9% at $\dot{m}_r = 6$, whereas the pressure losses is still relatively low (0.91 kPa). The obtained relative humidity of the outlet air is almost 100%.

(d) The multi-stage bubble column humidifier shows a higher effectiveness compared with the packed bed humidifier.

(e) Although the minimum effectiveness is at $\dot{m}_r = 4$, the maximum GOR obtained is at this point since it corresponds to $\mathrm{HCR}_H \approx 1$. So, it is very important to enhance the humidifier's effectiveness at the optimum mass ratio (where $\mathrm{HCR}_H = 1$).

4.2 Future scope

1. Heating the water entering the system by recovering some heat from the exhausted air.

2. Enhancing the effectiveness of the humidifier at $\mathrm{HCR}_H = 1$ by adding more stages.

3. Investigating the effect of top brine temperature (temperature of water entering the humidifier) .

4. Investigating the effect of inlet air relative humidity.

5. Using saline water.

APPENDICES

APPENDIX A

ORIFICE METER DESIGN

An orifice meter is a device used for measuring either mass or volumetric flow rate. It uses Bernoulli's principle which states that the pressure of the fluid is inversely proportional to its velocity. The orifice meter is constructed of a thin circular plate with a sharp edged hole at its center. The plate is placed between two flanges with gaskets. ISO 5167 [38] is used in order to design and install the orifice meter.

Since the orifice meter is to be located close to a blower which is a swirl inducing device, adding a straightener upstream is essential. The straightener consists of a bundle of tubes. Figure A.1 indicates the minimum acceptable distance of the straightener from the orifice plate.

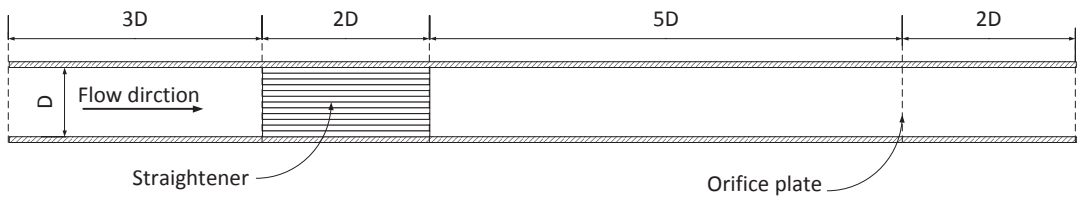

Figure. A.1: Minimum distance of the straightener from the orifice plate.

There are three types of tappings, that is, where the pressure difference is measured. These three types are flange, corner and d&d/2 tappings. In this work, d&d/2 tapping is used as shown in Figure A.2.

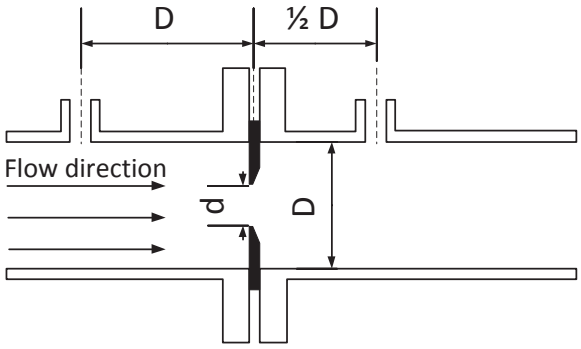

Figure. A.2: D and 1/2 D tapping orifice meter.

In this work, the orifice meter is used in order to measure the volumetric flow rate of the air stream as shown in Figure A.2. The orifice meter is a differential pressure meter which operates based on Bernoulli's equation. Hence the volumetric flow rate can be expressed as:

$$\dot{\forall} = C_d \cdot \frac{\frac{\pi}{4} D^2}{\sqrt{1 - (D^2/d^2)^2}} \cdot \sqrt{\frac{2\, g\, \rho_w\, \Delta z}{\rho_a}} \tag{A.1}$$

where C_d is a discharge coefficient which is considered due to various losses (sudden change in the flow area, friction losses, etc.). In general, the discharge coefficient for the orifice meter is a function of Reynolds number as well as the diameter ratio ($\beta = d/D$). However, C_d becomes independent of Reynolds number at high values of Reynolds number. Based on ISO 5167 [38], C_d is calculated using the following equation:

$$C_d = 0.5959 + 0.0312\,\beta^{2.1} - 0.184\,\beta^8 - 0.01685\,\beta^3 + \\ + 0.09\,\frac{\beta^4}{1-\beta^4} + 0.0029\,\beta^{2.5}\left(\frac{10^6}{Re}\right)^{0.75} \tag{A.2}$$

APPENDIX B

TURBOCHARGER

The GT2252 turbocharger is selected to be used in the thermodynamic analysis [39]. This turbocharger is manufactured by Garrett. Figure B.1 illustrates the performance map of the GT2252 turbocharger.

From the performance chart, the compressor efficiency is evaluated as follows:

$$\eta_c = \begin{cases} -88Pr^2 + 263Pr - 120 & \text{if} \quad Pr < 1.447 \\ 78 & \text{if} \quad Pr \geq 1.447 \end{cases} \tag{B.1}$$

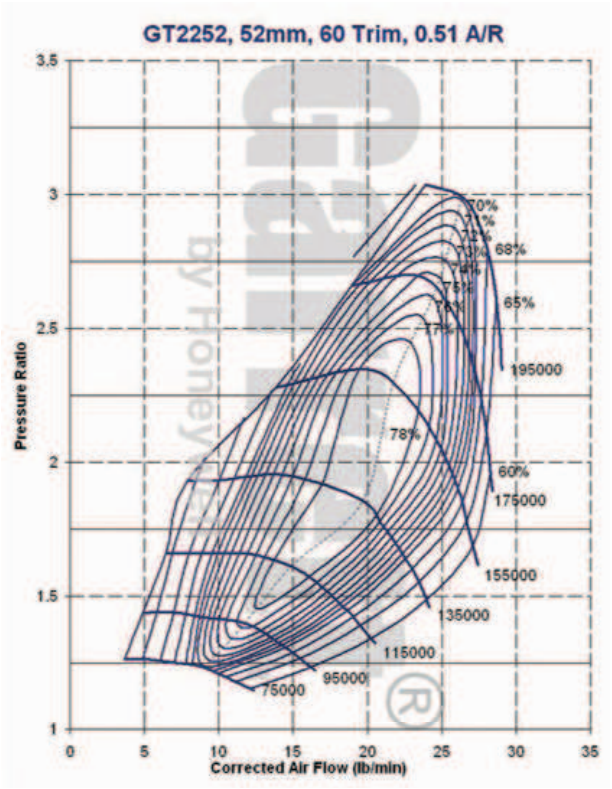

Figure. B.1: Performance map of GT2252 turbocharger [39].

APPENDIX C

UNCERTAINTY ANALYSIS

This appendix summarizes the approach used to evaluate the uncertainty in the experimental measurements. The following equation is used as a propagation equation of 95% confidence intervals,

$$U_r^2 = B_r^2 + P_r^2 \tag{C.1}$$

with a symmetric bias of the result calculated by

$$B_r^2 = \sum_{i=1}^{N} \left(\frac{\partial R}{\partial X_i} \right)^2 B_{X_i}^2 + \sum_{i=1}^{N} \sum_{j=1}^{N} 2 \left(\frac{\partial R}{\partial X_i} \right) \left(\frac{\partial R}{\partial X_j} \right) B_{X_i}^{'} B_{X_j}^{'} (1 - \delta_{ij}) \tag{C.2}$$

and the precession uncertainty of the result calculated by

$$P_r^2 = \sum_{i=1}^{N} \left(\frac{\partial R}{\partial X_i} \right)^2 P_{X_i}^2 \tag{C.3}$$

where

U_r is the total uncertainty error.

B_r is the total bias error.

P_r is the total precession error.

R is the reduction equation.

X is the measured variable.

B'_{X_i} and B'_{X_j} are the correlated bias errors.

$\frac{\partial R}{\partial X_i}$ is the sensitivity of the measured variable.

C.1 Thermocouples and data logger calibration

The thermocouples used to measure the dry and wet temperatures of the inlet and outlet air were calibrated together at the same time using the same data logger and bath of water. A liquid-in-glass thermometer with accuracy of ±0.5°C was used as a reference during the calibration. The calibrations were conducted at 0.0, 20.0 and 46.5°C. Curve fitting equations are used to evaluate the actual temperatures as shown in Figure C.1.

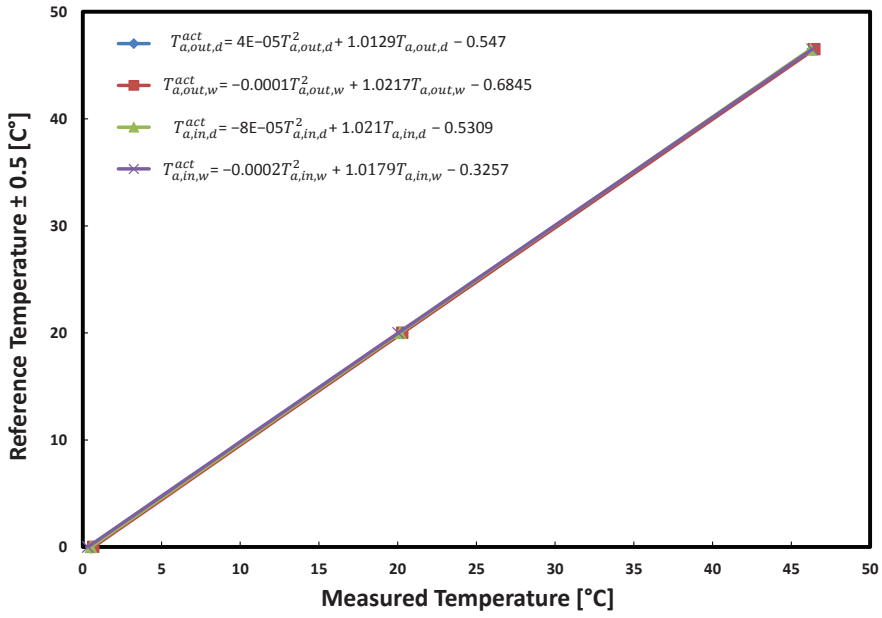

Figure. C.1: Calibration curves of $T_{a,in,dry}$, $T_{a,in,wet}$, $T_{a,out,dry}$ and $T_{a,out,wet}$.

The same was applied to the thermocouples used to measure the inlet and outlet water temperatures. Figure C.2 shows the curve fitting equations used to evaluate the actual temperatures.

The calibration reduced the bias error provided by the manufacturer from 2.2°C for the thermocouples and $1\% \pm 0.7$°C for the data logger to ±0.5°C for the

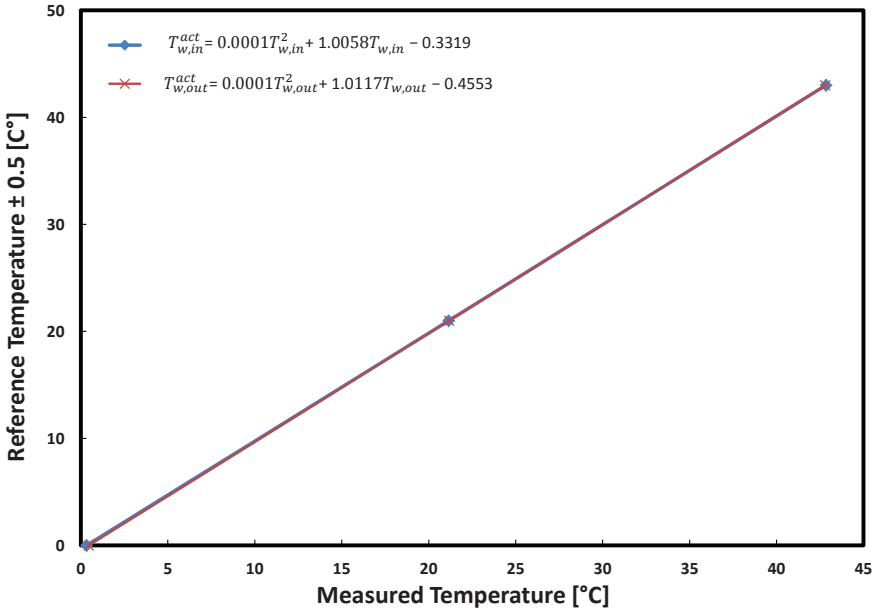

Figure. C.2: Calibration curves of $T_{w,in}$ and $T_{w,out}$.

combination of the thermocouple and data logger. Also, since the temperatures were measured using the same device, the bias limit for $T_{a,in,dry}$, $T_{a,in,wet}$, $T_{a,out,dry}$ and $T_{a,out,wet}$ as well as $T_{w,in}$ and $T_{w,out}$ are correlated.

C.2 Uncertainty analysis tables

The calculations of the uncertainties for V_{SG}, $\dot{m}_r$, ϕ_{in}, ϕ_{out} and ε are listed in Tables C.1,C.2 and C.3 at $\dot{m}_r = 2$, 4 and 6, respectively.

Table. C.1: Uncertainty analysis at $\dot{m}_r = 2$

	Parameter	Unit	ΔX_i	$\left(\frac{\partial V}{\partial X_i}\right)$	P_{Xi}	$\left(\frac{\partial V}{\partial X_i}\right)^2 P_{Xi}^2$	B_{Xi}	$\left(\frac{\partial V}{\partial X_i}\right)^2 B_{Xi}^2$
Air superficial velocity uncertainty	$\dot{V}_{w,in}$	LPM	0.2	0	0.071	0.000	0.250	0.000
	ΔH_{orific}	$m\ H_2O$	0.002	30	0.003	0.009	0.000	0.000
	$\Delta H_{drop,dry}$	$m\ H_2O$	0.002	0	0.001	0.000	0.000	0.000
	$\Delta H_{drop,wet}$	$m\ H_2O$	0.002	0	0.001	0.000	0.000	0.000
	$T_{a,in,dry}$	°C	0.2	0.05	0.112	0.000	0.500	0.001
	$T_{a,in,wet}$	°C	0.2	0	0.112	0.000	0.500	0.000
	$T_{a,out,dry}$	°C	0.2	0	0.112	0.000	0.500	0.000
	$T_{a,out,wet}$	°C	0.2	0	0.112	0.000	0.500	0.000
	$T_{w,in}$	°C	0.2	0	0.112	0.000	0.500	0.000
	$T_{w,out}$	°C	0.2	0	0.112	0.000	0.500	0.000
	Cd	-	0.0122	53.2786885	0.000	0.000	0.012	0.423
						P_r=	0.095	cm/s
						B_r=	0.650	cm/s
						U_r=	0.657	cm/s
Mass flow rate ratio uncertainty	Parameter	Unit	ΔX_i	$\left(\frac{\partial \dot{m}_r}{\partial X_i}\right)$	P_{Xi}	$\left(\frac{\partial \dot{m}_r}{\partial X_i}\right)^2 P_{Xi}^2$	B_{Xi}	$\left(\frac{\partial \dot{m}_r}{\partial X_i}\right)^2 B_{Xi}^2$
	$\dot{V}_{w,in}$	LPM	0.2	0.925	0.071	0.004	0.250	0.053
	ΔH_{orific}	$m\ H_2O$	0.002	-2.5	0.003	0.000	0.000	0.000
	$\Delta H_{drop,dry}$	$m\ H_2O$	0.002	0	0.001	0.000	0.000	0.000
	$\Delta H_{drop,wet}$	$m\ H_2O$	0.002	-0.5	0.001	0.000	0.000	0.000
	$T_{a,in,dry}$	°C	0.2	0	0.112	0.000	0.500	0.000
	$T_{a,in,wet}$	°C	0.2	0	0.112	0.000	0.500	0.000
	$T_{a,out,dry}$	°C	0.2	0	0.112	0.000	0.500	0.000
	$T_{a,out,wet}$	°C	0.2	0	0.112	0.000	0.500	0.000
	$T_{w,in}$	°C	0.2	-0.005	0.112	0.000	0.500	0.000
	$T_{w,out}$	°C	0.2	0	0.112	0.000	0.500	0.000
	Cd	-	0.0122	-11.4754098	0.000	0.000	0.012	0.020
						P_r=	0.066	kg/s
						B_r=	0.270	kg/s
						U_r=	0.278	kg/s
Inlet relative humidity uncertainty	Parameter	Unit	ΔX_i	$\left(\frac{\partial \varphi_{in}}{\partial X_i}\right)$	P_{Xi}	$\left(\frac{\partial \varphi_{in}}{\partial X_i}\right)^2 P_{Xi}^2$	B_{Xi}	$\left(\frac{\partial \varphi_{in}}{\partial X_i}\right)^2 B_{Xi}^2$
	$\dot{V}_{w,in}$	LPM	0.2	0	0.071	0.000	0.250	0.000
	ΔH_{orific}	$m\ H_2O$	0.002	0	0.003	0.000	0.000	0.000
	$\Delta H_{drop,dry}$	$m\ H_2O$	0.002	0	0.001	0.000	0.000	0.000
	$\Delta H_{drop,wet}$	$m\ H_2O$	0.002	-5	0.001	0.000	0.000	0.000
	$T_{a,in,dry}$	°C	0.2	-3.1	0.112	0.120	0.500	2.402
	$T_{a,in,wet}$	°C	0.2	4.25	0.112	0.226	0.500	4.516
	$T_{a,out,dry}$	°C	0.2	0	0.112	0.000	0.500	0.000
	$T_{a,out,wet}$	°C	0.2	0	0.112	0.000	0.500	0.000
	$T_{w,in}$	°C	0.2	0	0.112	0.000	0.500	0.000
	$T_{w,out}$	°C	0.2	0	0.112	0.000	0.500	0.000
	Cd	-	0.0122	0	0.000	0.000	0.012	0.000
						P_r=	0.588	%
						B_r=	0.575	%
						U_r=	0.823	%
Outlet relative humidity uncertainty	Parameter	Unit	ΔX_i	$\left(\frac{\partial \varphi_{out}}{\partial X_i}\right)$	P_{Xi}	$\left(\frac{\partial \varphi_{out}}{\partial X_i}\right)^2 P_{Xi}^2$	B_{Xi}	$\left(\frac{\partial \varphi_{out}}{\partial X_i}\right)^2 B_{Xi}^2$
	$\dot{V}_{w,in}$	LPM	0.2	0	0.071	0.000	0.250	0.000
	ΔH_{orific}	$m\ H_2O$	0.002	0	0.003	0.000	0.000	0.000
	$\Delta H_{drop,dry}$	$m\ H_2O$	0.002	0	0.001	0.000	0.000	0.000
	$\Delta H_{drop,wet}$	$m\ H_2O$	0.002	0	0.001	0.000	0.000	0.000
	$T_{a,in,dry}$	°C	0.2	0	0.112	0.000	0.500	0.000
	$T_{a,in,wet}$	°C	0.2	0	0.112	0.000	0.500	0.000
	$T_{a,out,dry}$	°C	0.2	5.25	0.112	0.345	0.500	6.891
	$T_{a,out,wet}$	°C	0.2	-5.4	0.112	0.364	0.500	7.290
	$T_{w,in}$	°C	0.2	0	0.112	0.000	0.500	0.000
	$T_{w,out}$	°C	0.2	0	0.112	0.000	0.500	0.000
	Cd	-	0.0122	0	0.000	0.000	0.012	0.000
						P_r=	0.842	%
						B_r=	0.075	%
						U_r=	0.845	%
Effectiveness uncertainty	Parameter	Unit	ΔX_i	$\left(\frac{\partial \varepsilon}{\partial X_i}\right)$	P_{Xi}	$\left(\frac{\partial \varepsilon}{\partial X_i}\right)^2 P_{Xi}^2$	B_{Xi}	$\left(\frac{\partial \varepsilon}{\partial X_i}\right)^2 B_{Xi}^2$
	$\dot{V}_{w,in}$	LPM	0.2	0.25	0.071	0.000	0.250	0.004
	ΔH_{orific}	$m\ H_2O$	0.002	0	0.003	0.000	0.000	0.000
	$\Delta H_{drop,dry}$	$m\ H_2O$	0.002	0	0.001	0.000	0.000	0.000
	$\Delta H_{drop,wet}$	$m\ H_2O$	0.002	0	0.001	0.000	0.000	0.000
	$T_{a,in,dry}$	°C	0.2	-3.35	0.112	0.140	0.500	2.806
	$T_{a,in,wet}$	°C	0.2	0.05	0.112	0.000	0.500	0.001
	$T_{a,out,dry}$	°C	0.2	0	0.112	0.000	0.500	0.000
	$T_{a,out,wet}$	°C	0.2	0	0.112	0.000	0.500	0.000
	$T_{w,in}$	°C	0.2	-0.2	0.112	0.000	0.500	0.010
	$T_{w,out}$	°C	0.2	3.65	0.112	0.167	0.500	3.331
	Cd	-	0.0122	0	0.000	0.000	0.012	0.000
						P_r=	0.555	%
						B_r=	2.388	%
						U_r=	2.451	%

Correlated Bias terms: $2\left(\frac{\partial R}{\partial X_i}\right)\left(\frac{\partial R}{\partial X_j}\right)B'_{X_i}B'_{X_j}$

-6.5875

-14.175

-0.08375

-0.365

Table. C.2: Uncertainty analysis at $\dot{m}_r = 4$

	Parameter	Unit	ΔX_i	$\left(\frac{\partial V}{\partial X_i}\right)$	P_{Xi}	$\left(\frac{\partial V}{\partial X_i}\right)^2 P_{Xi}^2$	B_{Xi}	$\left(\frac{\partial V}{\partial X_i}\right)^2 B_{Xi}^2$
Air superficial velocity uncertainty	$\dot{V}_{w,in}$	LPM	0.2	0	0.071	0.000	0.250	0.000
	ΔH_{orific}	$m\ H_2O$	0.002	30	0.003	0.009	0.000	0.000
	$\Delta H_{drop,dry}$	$m\ H_2O$	0.002	0	0.001	0.000	0.000	0.000
	$\Delta H_{drop,wet}$	$m\ H_2O$	0.002	0	0.001	0.000	0.000	0.000
	$T_{a,in,dry}$	°C	0.2	0.05	0.112	0.000	0.500	0.001
	$T_{a,in,wet}$	°C	0.2	0	0.112	0.000	0.500	0.000
	$T_{a,out,dry}$	°C	0.2	0	0.112	0.000	0.500	0.000
	$T_{a,out,wet}$	°C	0.2	0	0.112	0.000	0.500	0.000
	$T_{w,in}$	°C	0.2	0	0.112	0.000	0.500	0.000
	$T_{w,out}$	°C	0.2	0	0.112	0.000	0.500	0.000
	Cd	-	0.01	54	0.000	0.000	0.012	0.434
						$P_r =$	0.095	cm/s
						$B_r =$	0.659	cm/s
						$U_r =$	0.666	cm/s
Mass flow rate ratio uncertainty	Parameter	Unit	ΔX_i	$\left(\frac{\partial \dot{m}_r}{\partial X_i}\right)$	P_{Xi}	$\left(\frac{\partial \dot{m}_r}{\partial X_i}\right)^2 P_{Xi}^2$	B_{Xi}	$\left(\frac{\partial \dot{m}_r}{\partial X_i}\right)^2 B_{Xi}^2$
	$\dot{V}_{w,in}$	LPM	0.2	0.93	0.071	0.004	0.250	0.054
	ΔH_{orific}	$m\ H_2O$	0.002	-4.5	0.003	0.000	0.000	0.000
	$\Delta H_{drop,dry}$	$m\ H_2O$	0.002	0	0.001	0.000	0.000	0.000
	$\Delta H_{drop,wet}$	$m\ H_2O$	0.002	0	0.001	0.000	0.000	0.000
	$T_{a,in,dry}$	°C	0.2	0.01	0.112	0.000	0.500	0.000
	$T_{a,in,wet}$	°C	0.2	0	0.112	0.000	0.500	0.000
	$T_{a,out,dry}$	°C	0.2	0	0.112	0.000	0.500	0.000
	$T_{a,out,wet}$	°C	0.2	0	0.112	0.000	0.500	0.000
	$T_{w,in}$	°C	0.2	0	0.112	0.000	0.500	0.000
	$T_{w,out}$	°C	0.2	0	0.112	0.000	0.500	0.000
	Cd	-	0.01	-10.1	0.000	0.000	0.012	0.015
						$P_r =$	0.067	kg/s
						$B_r =$	0.263	kg/s
						$U_r =$	0.272	kg/s
Inlet relative humidity uncertainty	Parameter	Unit	ΔX_i	$\left(\frac{\partial \varphi_{in}}{\partial X_i}\right)$	P_{Xi}	$\left(\frac{\partial \varphi_{in}}{\partial X_i}\right)^2 P_{Xi}^2$	B_{Xi}	$\left(\frac{\partial \varphi_{in}}{\partial X_i}\right)^2 B_{Xi}^2$
	$\dot{V}_{w,in}$	LPM	0.2	0	0.071	0.000	0.250	0.000
	ΔH_{orific}	$m\ H_2O$	0.002	0	0.003	0.000	0.000	0.000
	$\Delta H_{drop,dry}$	$m\ H_2O$	0.002	0	0.001	0.000	0.000	0.000
	$\Delta H_{drop,wet}$	$m\ H_2O$	0.002	-5	0.001	0.000	0.000	0.000
	$T_{a,in,dry}$	°C	0.2	-2.6	0.112	0.084	0.500	1.690
	$T_{a,in,wet}$	°C	0.2	3.7	0.112	0.171	0.500	3.423
	$T_{a,out,dry}$	°C	0.2	0	0.112	0.000	0.500	0.000
	$T_{a,out,wet}$	°C	0.2	0	0.112	0.000	0.500	0.000
	$T_{w,in}$	°C	0.2	0	0.112	0.000	0.500	0.000
	$T_{w,out}$	°C	0.2	0	0.112	0.000	0.500	0.000
	Cd	-	0.01	0	0.000	0.000	0.012	0.000
						$P_r =$	0.506	%
						$B_r =$	0.550	%
						$U_r =$	0.747	%
Outlet relative humidity uncertainty	Parameter	Unit	ΔX_i	$\left(\frac{\partial \varphi_{out}}{\partial X_i}\right)$	P_{Xi}	$\left(\frac{\partial \varphi_{out}}{\partial X_i}\right)^2 P_{Xi}^2$	B_{Xi}	$\left(\frac{\partial \varphi_{out}}{\partial X_i}\right)^2 B_{Xi}^2$
	$\dot{V}_{w,in}$	LPM	0.2	0	0.071	0.000	0.250	0.000
	ΔH_{orific}	$m\ H_2O$	0.002	0	0.003	0.000	0.000	0.000
	$\Delta H_{drop,dry}$	$m\ H_2O$	0.002	0	0.001	0.000	0.000	0.000
	$\Delta H_{drop,wet}$	$m\ H_2O$	0.002	0	0.001	0.000	0.000	0.000
	$T_{a,in,dry}$	°C	0.2	0	0.112	0.000	0.500	0.000
	$T_{a,in,wet}$	°C	0.2	0	0.112	0.000	0.500	0.000
	$T_{a,out,dry}$	°C	0.2	5.05	0.112	0.319	0.500	6.376
	$T_{a,out,wet}$	°C	0.2	-5.15	0.112	0.332	0.500	6.631
	$T_{w,in}$	°C	0.2	0	0.112	0.000	0.500	0.000
	$T_{w,out}$	°C	0.2	0	0.112	0.000	0.500	0.000
	Cd	-	0.01	0	0.000	0.000	0.012	0.000
						$P_r =$	0.806	%
						$B_r =$	0.050	%
						$U_r =$	0.808	%
Effectiveness uncertainty	Parameter	Unit	ΔX_i	$\left(\frac{\partial \varepsilon}{\partial X_i}\right)$	P_{Xi}	$\left(\frac{\partial \varepsilon}{\partial X_i}\right)^2 P_{Xi}^2$	B_{Xi}	$\left(\frac{\partial \varepsilon}{\partial X_i}\right)^2 B_{Xi}^2$
	$\dot{V}_{w,in}$	LPM	0.2	0.35	0.071	0.001	0.250	0.008
	ΔH_{orific}	$m\ H_2O$	0.002	0	0.003	0.000	0.000	0.000
	$\Delta H_{drop,dry}$	$m\ H_2O$	0.002	0	0.001	0.000	0.000	0.000
	$\Delta H_{drop,wet}$	$m\ H_2O$	0.002	0	0.001	0.000	0.000	0.000
	$T_{a,in,dry}$	°C	0.2	-3.4	0.112	0.144	0.500	2.890
	$T_{a,in,wet}$	°C	0.2	0.05	0.112	0.000	0.500	0.001
	$T_{a,out,dry}$	°C	0.2	0	0.112	0.000	0.500	0.000
	$T_{a,out,wet}$	°C	0.2	-0.1	0.112	0.000	0.500	0.003
	$T_{w,in}$	°C	0.2	-0.8	0.112	0.008	0.500	0.160
	$T_{w,out}$	°C	0.2	4.25	0.112	0.226	0.500	4.516
	Cd	-	0.01	0	0.000	0.000	0.012	0.000
						$P_r =$	0.616	%
						$B_r =$	2.441	%
						$U_r =$	2.518	%

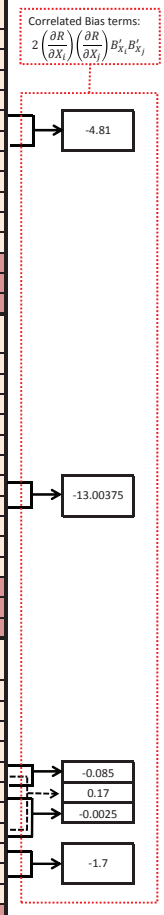

Table. C.3: Uncertainty analysis at $\dot{m}_r = 6$

	Parameter	Unit	ΔX_i	$\left(\frac{\partial V}{\partial X_i}\right)$	P_{X_i}	$\left(\frac{\partial V}{\partial X_i}\right)^2 P_{X_i}^2$	B_{X_i}	$\left(\frac{\partial V}{\partial X_i}\right)^2 B_{X_i}^2$
Air superficial velocity uncertainty	$\dot{\forall}_{w,in}$	LPM	0.2	0	0.071	0.000	0.250	0.000
	ΔH_{orific}	$m\ H_2O$	0.002	30	0.003	0.009	0.000	0.000
	$\Delta H_{drop,dry}$	$m\ H_2O$	0.002	0	0.001	0.000	0.000	0.000
	$\Delta H_{drop,wet}$	$m\ H_2O$	0.002	0	0.001	0.000	0.000	0.000
	$T_{a,in,dry}$	°C	0.2	0.05	0.112	0.000	0.500	0.001
	$T_{a,in,wet}$	°C	0.2	0	0.112	0.000	0.500	0.000
	$T_{a,out,dry}$	°C	0.2	0	0.112	0.000	0.500	0.000
	$T_{a,out,wet}$	°C	0.2	0	0.112	0.000	0.500	0.000
	$T_{w,in}$	°C	0.2	0	0.112	0.000	0.500	0.000
	$T_{w,out}$	°C	0.2	0	0.112	0.000	0.500	0.000
	Cd	-	0.01	52	0.000	0.000	0.012	0.402
						P_r=	0.095	cm/s
						B_r=	0.635	cm/s
						U_r=	0.642	cm/s
Mass flow rate ratio uncertainty	Parameter	Unit	ΔX_i	$\left(\frac{\partial \dot{m}_r}{\partial X_i}\right)$	P_{X_i}	$\left(\frac{\partial \dot{m}_r}{\partial X_i}\right)^2 P_{X_i}^2$	B_{X_i}	$\left(\frac{\partial \dot{m}_r}{\partial X_i}\right)^2 B_{X_i}^2$
	$\dot{\forall}_{w,in}$	LPM	0.2	0.935	0.071	0.004	0.250	0.055
	ΔH_{orific}	$m\ H_2O$	0.002	-6.5	0.003	0.000	0.000	0.000
	$\Delta H_{drop,dry}$	$m\ H_2O$	0.002	0	0.001	0.000	0.000	0.000
	$\Delta H_{drop,wet}$	$m\ H_2O$	0.002	0	0.001	0.000	0.000	0.000
	$T_{a,in,dry}$	°C	0.2	0.01	0.112	0.000	0.500	0.000
	$T_{a,in,wet}$	°C	0.2	0	0.112	0.000	0.500	0.000
	$T_{a,out,dry}$	°C	0.2	0	0.112	0.000	0.500	0.000
	$T_{a,out,wet}$	°C	0.2	0	0.112	0.000	0.500	0.000
	$T_{w,in}$	°C	0.2	0	0.112	0.000	0.500	0.000
	$T_{w,out}$	°C	0.2	0	0.112	0.000	0.500	0.000
	Cd	-	0.01	-11.7	0.000	0.000	0.012	0.020
						P_r=	0.069	kg/s
						B_r=	0.274	kg/s
						U_r=	0.283	kg/s
Inlet relative humidity uncertainty	Parameter	Unit	ΔX_i	$\left(\frac{\partial \varphi_{in}}{\partial X_i}\right)$	P_{X_i}	$\left(\frac{\partial \varphi_{in}}{\partial X_i}\right)^2 P_{X_i}^2$	B_{X_i}	$\left(\frac{\partial \varphi_{in}}{\partial X_i}\right)^2 B_{X_i}^2$
	$\dot{\forall}_{w,in}$	LPM	0.2	0	0.071	0.000	0.250	0.000
	ΔH_{orific}	$m\ H_2O$	0.002	0	0.003	0.000	0.000	0.000
	$\Delta H_{drop,dry}$	$m\ H_2O$	0.002	0	0.001	0.000	0.000	0.000
	$\Delta H_{drop,wet}$	$m\ H_2O$	0.002	0	0.001	0.000	0.000	0.000
	$T_{a,in,dry}$	°C	0.2	-2.5	0.112	0.078	0.500	1.563
	$T_{a,in,wet}$	°C	0.2	3.65	0.112	0.167	0.500	3.331
	$T_{a,out,dry}$	°C	0.2	0	0.112	0.000	0.500	0.000
	$T_{a,out,wet}$	°C	0.2	0	0.112	0.000	0.500	0.000
	$T_{w,in}$	°C	0.2	0	0.112	0.000	0.500	0.000
	$T_{w,out}$	°C	0.2	0	0.112	0.000	0.500	0.000
	Cd	-	0.01	0	0.000	0.000	0.012	0.000
						P_r=	0.495	%
						B_r=	0.575	%
						U_r=	0.758	%
Outlet relative humidity uncertainty	Parameter	Unit	ΔX_i	$\left(\frac{\partial \varphi_{out}}{\partial X_i}\right)$	P_{X_i}	$\left(\frac{\partial \varphi_{out}}{\partial X_i}\right)^2 P_{X_i}^2$	B_{X_i}	$\left(\frac{\partial \varphi_{out}}{\partial X_i}\right)^2 B_{X_i}^2$
	$\dot{\forall}_{w,in}$	LPM	0.2	0	0.071	0.000	0.250	0.000
	ΔH_{orific}	$m\ H_2O$	0.002	0	0.003	0.000	0.000	0.000
	$\Delta H_{drop,dry}$	$m\ H_2O$	0.002	0	0.001	0.000	0.000	0.000
	$\Delta H_{drop,wet}$	$m\ H_2O$	0.002	0	0.001	0.000	0.000	0.000
	$T_{a,in,dry}$	°C	0.2	0	0.112	0.000	0.500	0.000
	$T_{a,in,wet}$	°C	0.2	0	0.112	0.000	0.500	0.000
	$T_{a,out,dry}$	°C	0.2	5.05	0.112	0.319	0.500	6.376
	$T_{a,out,wet}$	°C	0.2	-5	0.112	0.313	0.500	6.250
	$T_{w,in}$	°C	0.2	0	0.112	0.000	0.500	0.000
	$T_{w,out}$	°C	0.2	0	0.112	0.000	0.500	0.000
	Cd	-	0.01	0	0.000	0.000	0.012	0.000
						P_r=	0.795	%
						B_r=	0.025	%
						U_r=	0.795	%
Effectiveness uncertainty	Parameter	Unit	ΔX_i	$\left(\frac{\partial \varepsilon}{\partial X_i}\right)$	P_{X_i}	$\left(\frac{\partial \varepsilon}{\partial X_i}\right)^2 P_{X_i}^2$	B_{X_i}	$\left(\frac{\partial \varepsilon}{\partial X_i}\right)^2 B_{X_i}^2$
	$\dot{\forall}_{w,in}$	LPM	0.2	0	0.071	0.000	0.250	0.000
	ΔH_{orific}	$m\ H_2O$	0.002	0	0.003	0.000	0.000	0.000
	$\Delta H_{drop,dry}$	$m\ H_2O$	0.002	0	0.001	0.000	0.000	0.000
	$\Delta H_{drop,wet}$	$m\ H_2O$	0.002	0	0.001	0.000	0.000	0.000
	$T_{a,in,dry}$	°C	0.2	0	0.112	0.000	0.500	0.000
	$T_{a,in,wet}$	°C	0.2	0.1	0.112	0.000	0.500	0.003
	$T_{a,out,dry}$	°C	0.2	0	0.112	0.000	0.500	0.000
	$T_{a,out,wet}$	°C	0.2	-4.05	0.112	0.205	0.500	4.101
	$T_{w,in}$	°C	0.2	2.8	0.112	0.098	0.500	1.960
	$T_{w,out}$	°C	0.2	0	0.112	0.000	0.500	0.000
	Cd	-	0.01	0	0.000	0.000	0.012	0.000
						P_r=	0.551	%
						B_r=	2.421	%
						U_r=	2.483	%

Correlated Bias terms: $2\left(\frac{\partial R}{\partial X_i}\right)\left(\frac{\partial R}{\partial X_j}\right)B'_{X_i}B'_{X_j}$

-4.5625

-12.625

-0.2025

REFERENCES

[1] Hisham T. El-Dessouky and Hisham M. Ettouney. *Fundamentals of Salt Water Desalination*. Elsevier, 2002.

[2] G. Prakash Narayan, Mostafa H. Sharqawy, Edward K. Summers, John H. Lienhard, Syed M. Zubair, and M.A. Antar. "The potential of solar-driven humidification-dehumidification desalination for small-scale decentralized water production". In: *Renewable and Sustainable Energy Reviews* 14.4 (2010), pp. 1187 –1201.

[3] Philippe Rekacewicz. *Water Scarcity Index*. February 2006.

[4] G. Prakash Narayan, Mostafa H. Sharqawy, John H. Lienhard V, and Syed M. Zubair. "Thermodynamic analysis of humidification dehumidification desalination cycles". In: *Desalination and Water Treatment* 16.1-3 (2010), pp. 339–353.

[5] G.P. Narayan, R.K. McGovern, S.M. Zubair, and J.H. Lienhard V. "Variable pressure humidification dehumidification desalination system". In: Proc AJTEC; 2011. ASME/JSME 8th Thermal Engineering Joint conference: Hawaii.

[6] G. Prakash Narayan, Ronan K. McGovern, Syed M. Zubair, and John H. Lienhard V. "High-temperature-steam-driven, varied-pressure, humidification-dehumidification system coupled with reverse osmosis for energy-efficient seawater desalination". In: *Energy* 37.1 (2012), pp. 482 – 493.

[7] R.E. Treybal. *Mass transfer operations*. 3ed. NY: McGraw-Hill, 1980.

[8] F. Kreith and R.F. Bohem. *Direct-contact heat transfer*. Washington: Hemisphere Pub. Corp., 1988.

[9] S.C Bhattacharya, San Shwe Hla, and Hoang-Luang Pham. "A study on a multi-stage hybrid gasifier-engine system". In: *Biomass and Bioenergy* 21.6 (2001), pp. 445 –460.

[10] J. Orfi, M. Laplante, H. Marmouch, N. Galanis, B. Benhamou, S. Ben Nasrallah, and C.T. Nguyen. "Experimental and theoretical study of a humidification-dehumidification water desalination system using solar energy". In: *Desalination* 168 (2004), pp. 151 –159.

[11] Said Al-Hallaj, Mohammed Mehdi Farid, and Abdul Rahman Tamimi. "Solar desalination with a humidification-dehumidification cycle: performance of the unit". In: *Desalination* 120.3 (1998), pp. 273 –280.

[12] Y.J. Dai, R.Z. Wang, and H.F. Zhang. "Parametric analysis to improve the performance of a solar desalination unit with humidification and dehumidification". In: *Desalination* 142.2 (2002), pp. 107 –118.

[13] A.S. Nafey, H.E.S. Fath, S.O. El-Helaby, and A. Soliman. "Solar desalination using humidification-dehumidification processes. Part II. An experimental investigation". In: *Energy Conversion and Management* 45.78 (2004), pp. 1263 –1277.

[14] Ghazi Al-Enezi, Hisham Ettouney, and Nagla Fawzy. "Low temperature humidification dehumidification desalination process". In: *Energy Conversion and Management* 47.4 (2006), pp. 470 –484.

[15] G. Prakash Narayan, Maximus G. St. John, Syed M. Zubair, and John H. Lienhard V. "Thermal design of the humidification dehumidification desalination system: An experimental investigation". In: *International Journal of Heat and Mass Transfer* 58.12 (2013), pp. 740 –748.

[16] C.D. Cooper and F.C. Alley. *Air Pollution Control: A Design Approach*. Waveland Press, Incorporated, 2011.

[17] G.P. Narayan, M.H. Sharqawy, S. Lam, J.H. Lienhard V, and M. St. John. "Multistage bubble column humidifier". Pat. Application No. 13/916,038. To Be Filed 2014.

[18] S.A. El-Agouz and M. Abugderah. "Experimental analysis of humidification process by air passing through seawater". In: *Energy Conversion and Management* 49.12 (2008), pp. 3698 –3703.

[19] H.P. Garg, R.S. Adhikari, and Rakesh Kumar. "Experimental design and computer simulation of multi-effect humidification (MEH)-dehumidification solar distillation". In: *Desalination* 153.13 (2003), pp. 81 –86.

[20] Efat Chafik. “A new seawater desalination process using solar energy”. In: *Desalination* 153.13 (2003), pp. 25 –37.

[21] Efat Chafik. “A new type of seawater desalination plants using solar energy”. In: *Desalination* 156 (2003), pp. 333 –348.

[22] Mahmoud Ben Amara, Imed Houcine, Amenallah Guizani, and Mohammed Malej. “Experimental study of a multiple-effect humidification solar desalination technique”. In: *Desalination* 170.3 (2004), pp. 209 –221.

[23] S.A. El-Agouz. “Desalination based on humidification-dehumidification by air bubbles passing through brackish water”. In: *Chemical Engineering Journal* 165.2 (2010), pp. 413 –419.

[24] Lixi Zhang, Guangping Cheng, and Shiyuan Gao. “Experimental study on air bubbling humidification”. In: *Desalination and Water Treatment* 29.1-3 (2011), pp. 258–263.

[25] G. Prakash Narayan, Mostafa H. Sharqawy, Steven Lam, Sarit K. Das, and John H. Lienhard. “Bubble columns for condensation at high concentrations of noncondensable gas: Heat-transfer model and experiments”. In: *AIChE Journal* 59.5 (2013), pp. 1780–1790.

[26] G Prakash Narayan, Karan H Mistry, Mostafa H Sharqawy, Syed M Zubair, and John H Lienhard. “Energy Effectiveness of Simultaneous Heat and Mass Exchange Devices”. In: *Frontiers in Heat and Mass Transfer* 1.2 (2010), pp. 1–13.

[27] G. Prakash Narayan, John H. Lienhard V, and Syed M. Zubair. "Entropy generation minimization of combined heat and mass transfer devices". In: *International Journal of Thermal Sciences* 49.10 (2010), pp. 2057 –2066.

[28] S.A. Klein. ENGINEERING EQUATION SOLVER. *Academic Professional, Version 9.4*. Version 9.4. 2013.

[29] Karan H. Mistry, Alexander Mitsos, and John H. Lienhard V. "Optimal operating conditions and configurations for humidificationdehumidification desalination cycles". In: *International Journal of Thermal Sciences* 50.5 (2011), pp. 779 –789.

[30] Nigar Kantarci, Fahir Borak, and Kutlu O. Ulgen. "Bubble column reactors". In: *Process Biochemistry* 40.7 (2005), pp. 2263 –2283.

[31] A.A. Mouza, G.K. Dalakoglou, and S.V. Paras. "Effect of liquid properties on the performance of bubble column reactors with fine pore spargers". In: *Chemical Engineering Science* 60.5 (2005), pp. 1465 –1475.

[32] *Standard AS568 USA O-Ring Sizing Chart*. MARCO RUBBER & PLASTIC PRODUCTS, INC.

[33] *Industrial Groove Design Charts*. MARCO RUBBER & PLASTIC PRODUCTS, INC.

[34] Hugh W. Coleman and W. Glenn Steele. "Experimentation, Validation, and Uncertainty Analysis for Engineers, Third Edition". In: *Experimentation, Validation, and Uncertainty Analysis for Engineers*. John Wiley & Sons, Inc., 2009, pp. 257–269.

[35] U.Parasu Veera, K.L Kataria, and J.B Joshi. “Effect of superficial gas velocity on gas hold-up profiles in foaming liquids in bubble column reactors”. In: *Chemical Engineering Journal* 99.1 (2004), pp. 53 –58.

[36] Donald F. Elger, Barbara C. Williams, Clayton T. Crowe, and John A. Roberson. *Engineering Fluid Mechanics*. 10th ed. Wiley.

[37] G. Prakash Narayan, Maximus G. St. John, Syed M. Zubair, and John H. Lienhard V. “Thermal design of the humidification dehumidification desalination system: An experimental investigation”. In: *International Journal of Heat and Mass Transfer* 58 (2013), pp. 740 –748.

[38] *Measurement of fluid flow by means of pressure differential devices inserted in circular cross-section conduits running*. ISO5167.

[39] www.turbobygarrett.com. *GT2252*.

Vitae

- Name: Obaidallah Mohammad Ali Munteshari
- Nationality: Saudi Arabian
- Date of Birth: 18 February 1988
- Email: *obaidallah@kfupm.edu.sa* , *obaidallah.mu@gmail.com*
- Permenant Address: 1959 KFUPM, Dhahran, SA
- Education:

  M.Sc (Mechanical Engineering), April 2014, KFUPM.

  B.Sc (Mechanical Engineering), August 2011, KFUPM.